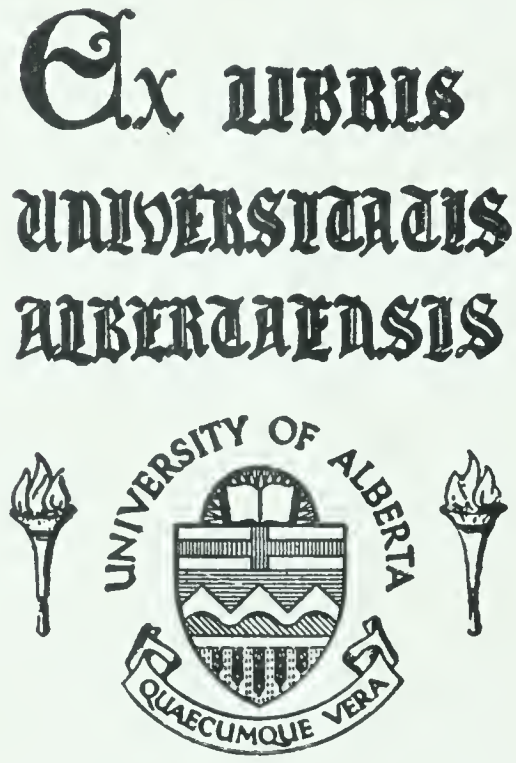

University of Alber
Printing Departme

THE UNIVERSITY OF ALBERTA

THE SEMICONDUCTOR JUNCTION DETECTOR APPLIED TO SOME ALPHA PARTICLE REACTIONS

by

CARY NATHAN DAVIDS

A THESIS

SUBMITTED TO THE FACULTY OF GRADUATE STUDIES

IN PARTIAL FULFILMENT OF THE REQUIREMENTS FOR THE DEGREE

OF MASTER OF SCIENCE

DEPARTMENT OF PHYSICS

EDMONTON, ALBERTA

SEPTEMBER, 1962

ABSTRACT

This thesis is divided into two major sections. In chapter I a fast neutron monitor is described which uses the pulse-shape discriminating properties of a liquid scintillator to make it insensitive to gamma radiation. The efficiency of the monitor as a function of neutron energy is given, followed by a discussion of the factors which influence the pulse-shape discrimination process.

Chapter II deals with the use of the semiconductor junction detector as a charged particle spectrometer. The experimental arrangement and target chamber are described. Basic characteristics of the detector are derived from the solution of Poisson's equation, and the effects of excessive charged particle bombardment on the resolution of a detector are shown to be small. A description of angular distribution measurements made on the reactions $F^{19}(p,\alpha_o)O^{16}$ and $F^{19}(p,\alpha_1)O^{16*}$ is followed by a preliminary analysis of the charged particle spectrum resulting from the bombardment of B^{11} by 0.5 MeV deuterons. Finally, recommendations for improving the apparatus are proposed.

ACKNOWLEDGEMENTS

I wish to express my gratitude to Dr. G. C. Neilson, my supervisor, and to Drs. W. K. Dawson and J. T. Sample for their help and encouragement during the course of this work.

Thanks are due to Mr. Con Green who did most of the machining, to Mr. Jock Elliott who helped with the drawings for this thesis, and to Mr. Max Burbank who did the programming for the computer calculations.

In addition, I am deeply indebted to Mr. Walter Davies for his constant and valuable aid throughout the period of this project.

A Bursary from the National Research Council of Canada is gratefully acknowledged.

Finally, I would like to thank Dr. W. T. Sharp for his helpful comments on the section dealing with angular distributions.

TABLE OF CONTENTS

LIST OF FIGURES

I. FAST NEUTRON MONITOR

1. Purpose -

Many experiments involving fast neutrons are being performed in the Van de Graaff laboratory at the University of Alberta, and a fast neutron monitor serves several purposes:

1) When placed a meter or so away from the target, it serves as a relative indicator of the beam current. For (d,n) and (p,n) reactions, the number of neutrons detected at some angle to the beam direction during a given time interval is proportional to the number of incident particles. Non-uniformities in the target can also be determined by the relative neutron yield at different target positions.

2) In the case of deuterium ice targets, a decrease in neutron yield indicates that the target temperature has been raised above -100° C., causing rapid vaporization. The relative yield of neutrons also indicates that the ice layer is suitably thick.

3) A crude estimate of the neutron flux in the target area for personnel protection is provided by the monitor. Its efficiency for neutrons is not constant with energy, however, and such an estimate can only be correct to within an order of magnitude.

2. Introduction -

When detecting the presence of fast neutrons, it is important to use a counter which is insensitive to gamma radiation. In most of the nuclear reactions of which fast neutrons are a product, gamma rays accompany the neutrons, and are also produced when the beam strikes various metal objects in its path. Of the various means by which fast neutrons may be detected, the scintillation counter is one of the most widely used because of its high efficiency. Of course, the scintillator must be chosen to contain a good percentage of hydrogen, since the neutron is observed only by the proton recoils from n-p scattering.

Unfortunately, such a scintillation counter also has a high efficiency for charged particles and gamma rays. Protons and heavier charged particles can be excluded from the detector by proper shielding. Electrons may be eliminated by a combination of shielding and keeping the detector a meter or two from the target. The gamma rays alone remain to cause the unwanted background. In addition, there will be neutrons originating from reactions occurring in the region between the accelerator and the target. Precautions

must be taken to remove this source of spurious counts. Proper shielding of the beam tube helps to lower this unwanted background.

Many techniques for neutron-gamma discrimination are discussed in the literature (Ma60)*. Coincidence methods, using a particle or gamma ray associated with the neutron, or using gating pulses from neutron insensitive scintillators like sodium iodide, have been used to reduce the gamma ray background. Special assemblies, like the Hornyak button and sandwich scintillators, have been used with varying degrees of success. Time-of-flight methods utilize the small time resolution of the instrumentation to eliminate much of the beam-associated background.

Recently a new technique has evolved, based on a phenomenon peculiar to certain organic scintillators (Wr56). It is found that the decay times of the scintillations from these materials increases with the specific ionization of the detected particle. Actually, it has been shown that the decay consists of a slow and a fast component, and it is the relative amounts of each which is determined by the nature of the ionizing particle. Thus the scintillations

* References will be found at the end of the thesis.

due to protons (caused by recoil from a neutron) and electrons (produced when the incident gamma rays undergo Compton scattering or the photoelectric effect) may be separated electronically using their different scintillation pulse shapes (Ow58).

Some scintillators which are useful for pulse-shape discrimination are stilbene, quaterphenyl, and anthracene. These are solid crystals. Certain liquid scintillators exhibit the same decay time characteristics, provided that all dissolved oxygen is first removed (Br59).

The utility of a neutron-gamma discriminator extends further than neutron monitor applications. In fast neutron spectroscopy, this technique has been used successfully to reduce the background due to low energy gamma rays. As a result, fewer random events are recorded, and less prominent neutron groups are more clearly observed (see for example, Li59, Ne60, An62).

In the present application, it was originally intended

to use a plastic phosphor (NE77)* as the scintillation material. This phosphor has the advantage of large size, and it is easily tested for discrimination using a Pu^{239} alpha source and any gamma source available in the laboratory. However, it was found that the difference in pulse shapes for alpha particles of 5.1 MeV and gamma rays of energy 2.62 MeV was too small to provide sensitive discrimination. Accordingly, a liquid scintillator was substituted (NE213)*, and it proved to have adequate discrimination properties, although it could not be tested with alpha particles.

3. Circuit Details -

The circuit chosen was that due to Daehnick and Sherr (Da61). (See figure I-1). Their original work had been done with a stilbene crystal, so in order to become familiar with the techniques, their whole assembly was duplicated. The photomultiplier tube was a fourteen stage RCA type 6810, with a stilbene crystal of dimensions 1 5/8 in. diameter by 1 1/8 in. deep. After adjustment, the circuit discriminated well between 5.1 MeV alpha particles and

* Nuclear Enterprises Ltd.(Canada), Winnipeg, Man.

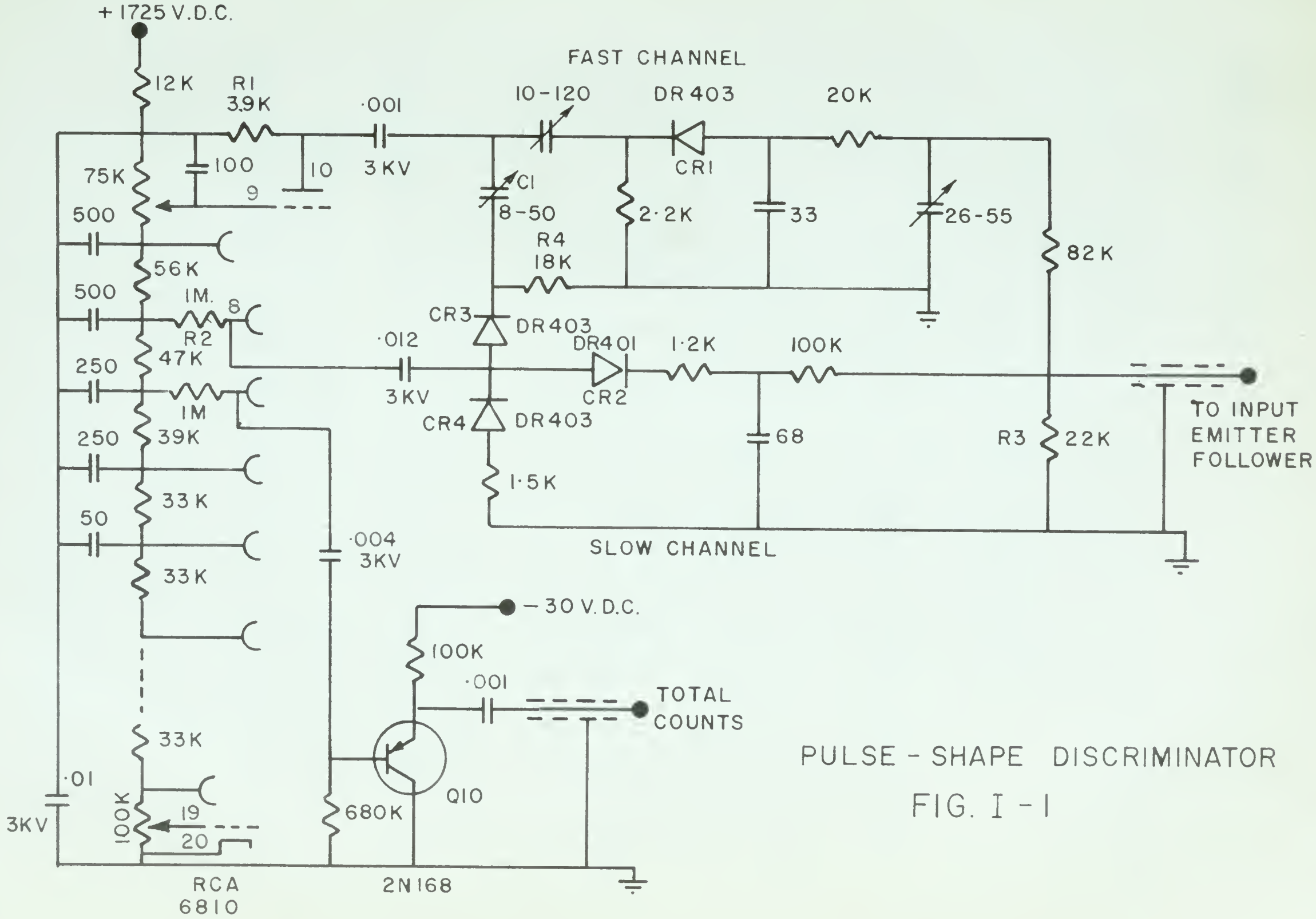

PULSE - SHAPE DISCRIMINATOR

FIG. I - 1

gamma rays up to 2.62 MeV.

The operation of the pulse shape discriminator is as follows. The current pulse through the photomultiplier may be approximated by the sum of two terms:

$$I(E,t) = I_o(E)\left[e^{-\frac{t}{\tau_f}} + a(E)e^{-\frac{t}{\tau_s}}\right] \qquad (1)$$

where τ_f is a fast decay time, $\lesssim$ 10 ns and τ_s is a slow decay time, usually several hundred ns*. The coefficient a depends on the specific ionization, dE/dx, of the charged particle which is actually detected. a is small for electrons (about 0.011 for several MeV) and increases for more heavily ionizing particles (about 0.021 for protons of similar energy) (Da61). It is the excess of slow component possessed by proton pulses which enables them to be separated from electron pulses.

The photomultiplier current pulse is integrated by stray capacities at the anode and at the second last dynode.

*Recent results (Al61) indicate that stilbene has an additional slow component approximately 1 μs in duration.

The anode capacity is discharged through a low resistance R_1 = 3.9 kohm (integrating time ~ 10^{-8} s), whereas the dynode capacity sees a 1 megohm resistance R_2 (integrating time several μs). As a consequence, the voltage pulse obtained from the anode consists of only a sharp negative spike lasting three or four μs. The dynode pulse is a positive pulse which contains a slowly decaying tail. Both pulses are stretched by means of solid state diodes, CR1 and CR2, and added together on a common load resistor R_3. The integrating time constants are adjusted so that gamma rays (electrons) produce a zero or negative output, while neutrons (protons) and heavily ionizing particles give a positive output pulse. The magnitude of this pulse depends on the photomultiplier voltages. For example, Pu^{239} alpha particles in stilbene gave approximately 0.5v with a phototube voltage of 2150v.

An additional feature of this circuit is the coupling network between the fast (anode) channel and the slow (dynode) channel. This consists of a trimming capacitor, C_1, a solid state diode, CR3, and a resistor R_4. It effectively short - circuits the slow channel to ground for the first few hundred ns after the arrival of a

pulse. In this way the pulse obtained from the slow channel contains no fast component.

Another function of this coupling network is to minimise the effect of pulse pile-up. Two pulses occuring within about 0.1 μs of each other will tend to combine slow components to form an output proportional to the time between them. The coupling network effectively cancels the first pulse by shorting out the slow channel and permitting the slow channel stray integrating capacity to collect only charge due to the second pulse's slow component. Any slow component from the first scintillation remaining after the cancellation will also be collected, but this small proportion of error is more than compensated by the protection against pulse pile-up provided by the network. Of course, high count rates will cause unavoidable pile-up in the scintillator itself. Daehnick and Sherr give the figure of 0.3 μs as the lower limit time separation of two scintillations which will not pile up in the discriminator.

Since the stilbene crystal was too small for efficient counting, a liquid scintillator was used for the final

detector. After installing the liquid scintillator, it was found that adequate discrimination did not occur for phototube voltages greater than 1750v. For higher voltages it was observed that the anode pulse limited and every detected particle produced a positive output pulse. With the phototube voltage low, its gain was reduced by about an order of magnitude, and it was therefore necessary to provide amplification of the pulses derived from the pulse-shape discriminator. Circuitry added is shown in figures I - 2 and 3 . It included a long-tailed pair transistor amplifier (Q_2 -Q_3), a grounded base stage (Q_5) to eliminate negative pulses due to gamma rays, and a transistor trigger circuit Q_7 - Q_8 (Go59) with a very stable threshold. Pulses arriving at the trigger circuit (due to neutrons from a Pu-Be source) had amplitudes from 2v up to 5v. It was found that a small positive over-shoot appeared on gamma ray pulses, and so only those pulses above 0.17v were accepted. The pulses from the trigger circuit were of sufficient magnitude to drive a 100 ohm cable through an emitter follower Q_9.

An NPN transistor (Q_{10}, Fig. I -1) emitter follower

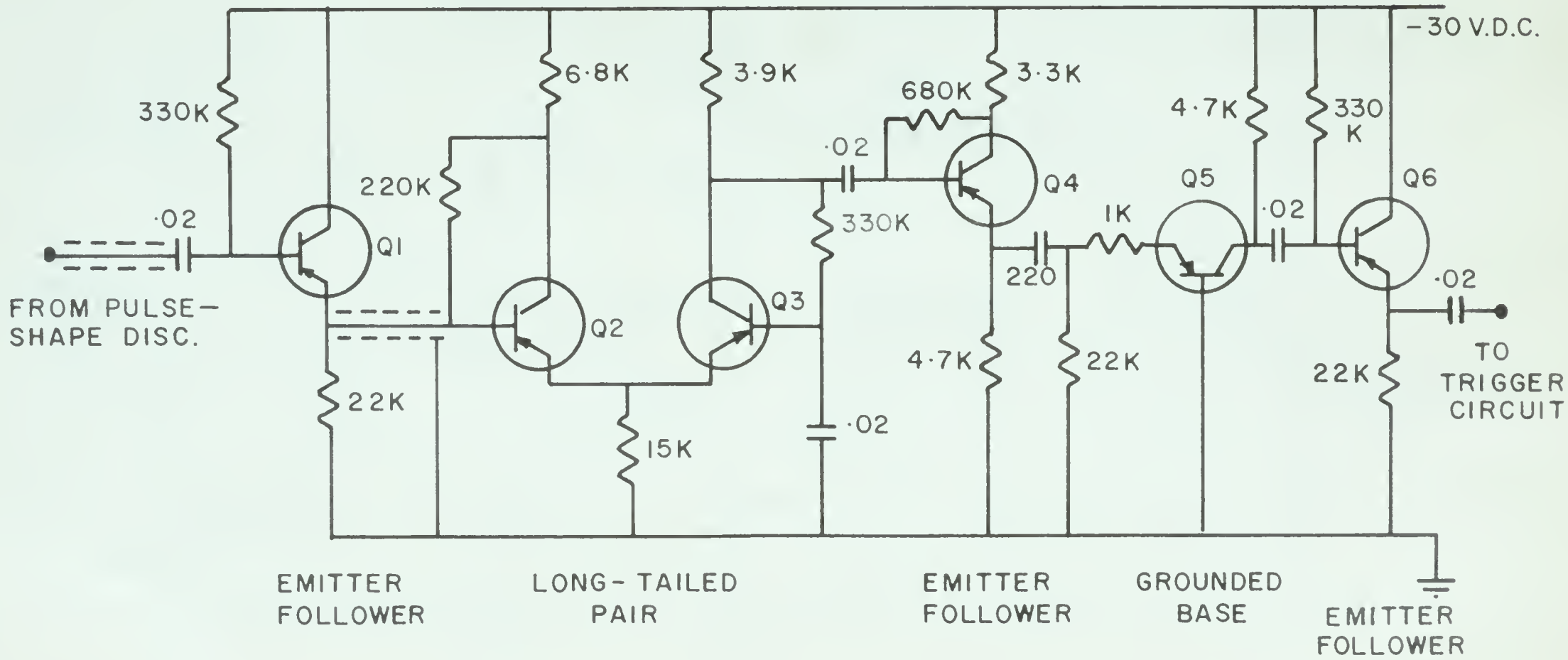
ALL TRANSISTORS 2N274
-30 V.D.C.
330K
6·8K
3·9K
680K
3·3K
4·7K
330 K
·02
220K
Q1
Q2
Q3
Q4
Q5
Q6
·02
330K
1K
·02
·02
FROM PULSE-SHAPE DISC.
220
22K
15K
·02
4·7K
22K
22K
TO TRIGGER CIRCUIT
EMITTER FOLLOWER
LONG-TAILED PAIR
EMITTER FOLLOWER
GROUNDED BASE
EMITTER FOLLOWER

FIG. I-2

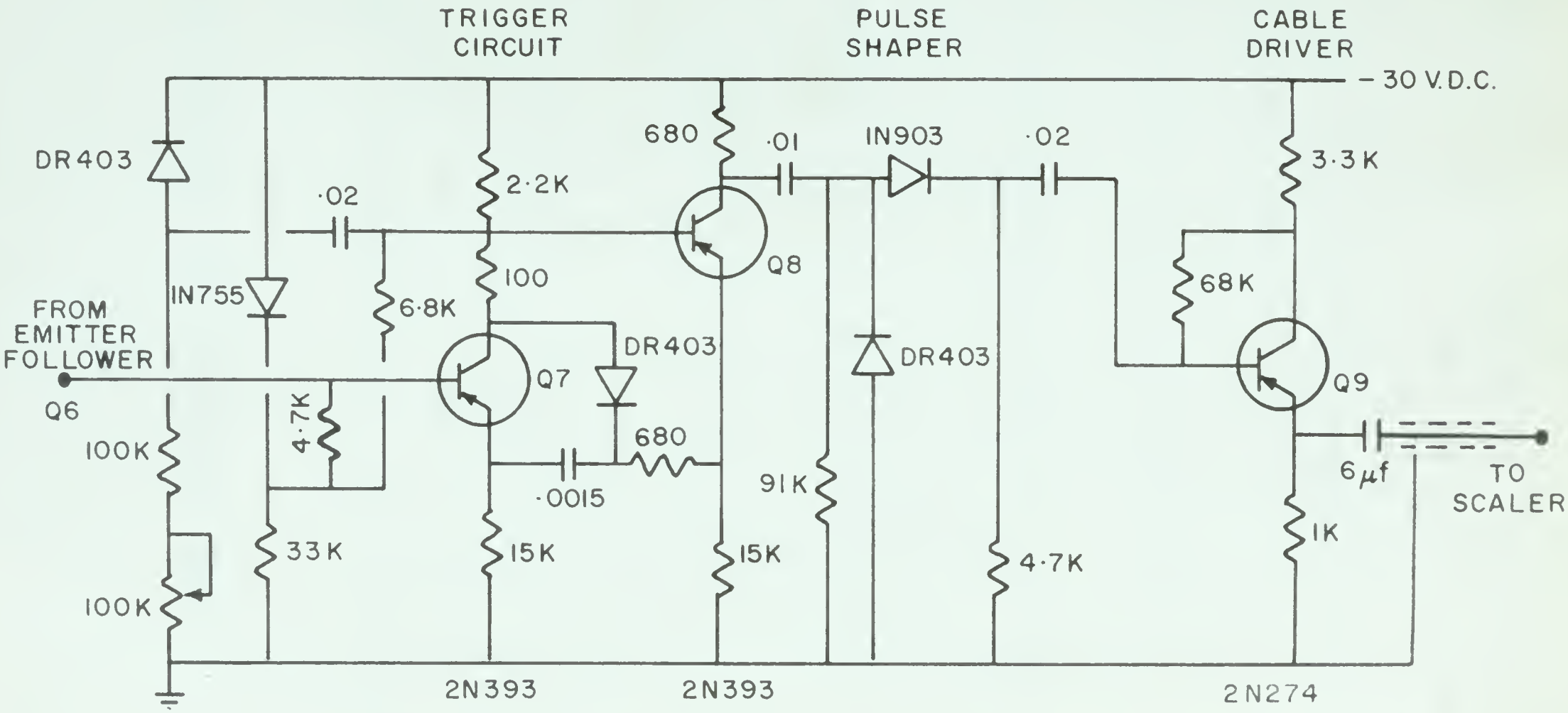
TRIGGER CIRCUIT
PULSE SHAPER
CABLE DRIVER
– 30 V.D.C.
DR403
·02
2·2K
680
·01
IN903
·02
3·3K
Q8
IN755
6·8K
100
68K
FROM EMITTER FOLLOWER
Q7
DR403
DR403
Q9
Q6
100K
4·7K
680
6 μf
TO SCALER
·0015
91K
33K
15K
15K
4·7K
1K
100K
2N393
2N393
2N274

FIG. I–3

was connected to the tenth dynode. Its output was coupled into a 100 ohm cable and fed to a scaler. Even with an arbitrary bias on the scaler, an estimate of the total count rate due to neutrons plus gamma rays was thus made available.

4. Test Runs and Efficiency Calculation -

The neutron monitor, using the liquid scintillator, was placed near the target of the Van de Graaff generator, and tested for response to high energy gamma rays. 6.1 MeV gamma rays from the reaction $F^{19}(p,\alpha)O^{16}*$ were used, coming from the 873 keV resonance. Pulses from the total counts output mentioned above were sent to a Model 204B Linear Amplifier*, whose discriminator output was coupled to a scaler. The discriminator threshold was set just above the noise, so that practically every detected gamma ray and neutron produced a scaler count. After subtracting background effects, it was found that the monitor responded to about one in every two thousand gamma

*Baird-Atomic, Inc., Cambridge, Mass.

scintillations. This figure corresponds to a count rate of about 5000 cts/min. High voltage setting was 1725 v.

An attempt was then made to determine the efficiency as a function of neutron energy of the monitor with respect to a paraffin-moderated BF_3 proportional counter. (A160). The long counter was placed at 125° to the beam direction, at a distance of 132 cm. The neutron monitor was mounted on a holder pivoting about the target center, permitting the measurement of the neutron angular distribution. The source of monoenergetic neutrons was the reaction $D(d,n)He^3$. The laboratory neutron angle was varied from 5° to 145° in intervals of ten degrees up to 65°, and of five degrees from 65° to 145°. Convenient tables of the laboratory differential cross-section for this reaction at various deuteron bombarding energies are available (Br60). The deuteron bombarding energy chosen was 1.43 MeV, so the Van de Graaff was set at 1.44 MeV, allowing 10 keV for the target thickness. Initially the target (a 1/16 inch gold plate, upon which was frozen a layer of deuterium oxide) was placed perpendicular to the beam direction. It was then rotated by 45°, in order to cover the region around 90°.

Corrections due to the absorption of neutrons by gold were applied to the data for neutron angles less than 70°, using the absorption cross-section from the 2nd edition of "Neutron Cross-Sections" (Hu60). This correction was 5% at most. Since the experimentally obtained quantity was to be the ratio of neutron monitor counts to long counter counts, no correction due to target thickness change under rotation was necessary.

The data from this experiment have been analysed in the following way. After the raw counts for both the long counter and the neutron monitor had been corrected for background and, where necessary, for gold absorption, the ratio $R(\theta) = \frac{\text{neutron monitor counts}}{\text{long counter counts}}$ was tabulated for all values of neutron angle θ. A crude estimate of the neutron detection efficiency for a hydrogenous liquid scintillator at neutron energy E_n is given by

$$\eta(E_n) = K\, \sigma_{np}(E_n) \cdot \frac{E_n - E_B}{E_n} \qquad (2)$$

where K is some normalization constant,

$\sigma_{np}(E_n)$ is the n-p cross-section at neutron energy E_n (Hu58),

E_B is the neutron bias, the lowest detectable

neutron energy (corresponding to the trigger circuit threshold)

and E_n is the neutron energy in the laboratory system. This expression assumes each neutron collides only once with a proton, and that the distribution of proton recoil energies is of the well-known rectangular form. Other factors not taken into consideration are losses by edge effects and gains caused by multiple collisons. Some of these events would be due to the carbon atoms, which are present roughly in the same proportion as hydrogen. Neilson et al (Ne60a) found the carbon effects, if any, to be within experimental error. It is expected that the geometrical distortions will be negligible in the present application, because of the small size of the scintillator (a cylinder 2" in diameter by 5" long).

The measured detection efficiency is given, to within a constant, by $$\eta'(E_n)\alpha \frac{R(E_n)}{\sigma(E_n)} \qquad (3)$$

where $R(E_n)$ is the same as $R(\theta)$ except that the energy of the neutron at angle θ is considered as the variable.

and $\sigma(E_n)$ is the differential cross-section for the

$D(d,n)He^3$ reaction as mentioned above.

We may now find the deviation from the crude efficiency by taking the ratio $\frac{\eta'(E_n)}{\eta(E_n)}$:

$$\frac{\eta'(E_n)}{\eta(E_n)} = B \frac{R(E_n)}{\sigma_{np}(E_n)\sigma(E_n)} \cdot \frac{E_n}{E_n - E_B} \qquad (4)$$

where B is a constant. The neutron bias E_B was chosen to be 1.70 MeV, by extrapolating the plot of $\eta'(E_n)$ vs neutron energy (fig. I-4) to zero efficiency. In figure I-4 the ratio $\frac{\eta'(E_n)}{\eta(E_n)}$ is also plotted against neutron energy.

5. Discussion -

In assessing the relative efficiency $\frac{\eta'(E_n)}{\eta(E_n)}$ one cannot give too much weight to the low energy points. This is because of the difficulty in assigning a value to the neutron bias E_B. A small change in this value would barely effect the high energy points but would shift the points for $E_n < 2.2$ MeV. Generally speaking, however, it seems that the response slowly increases up to 3.5 MeV, after which it begins to fall off, and more rapidly after

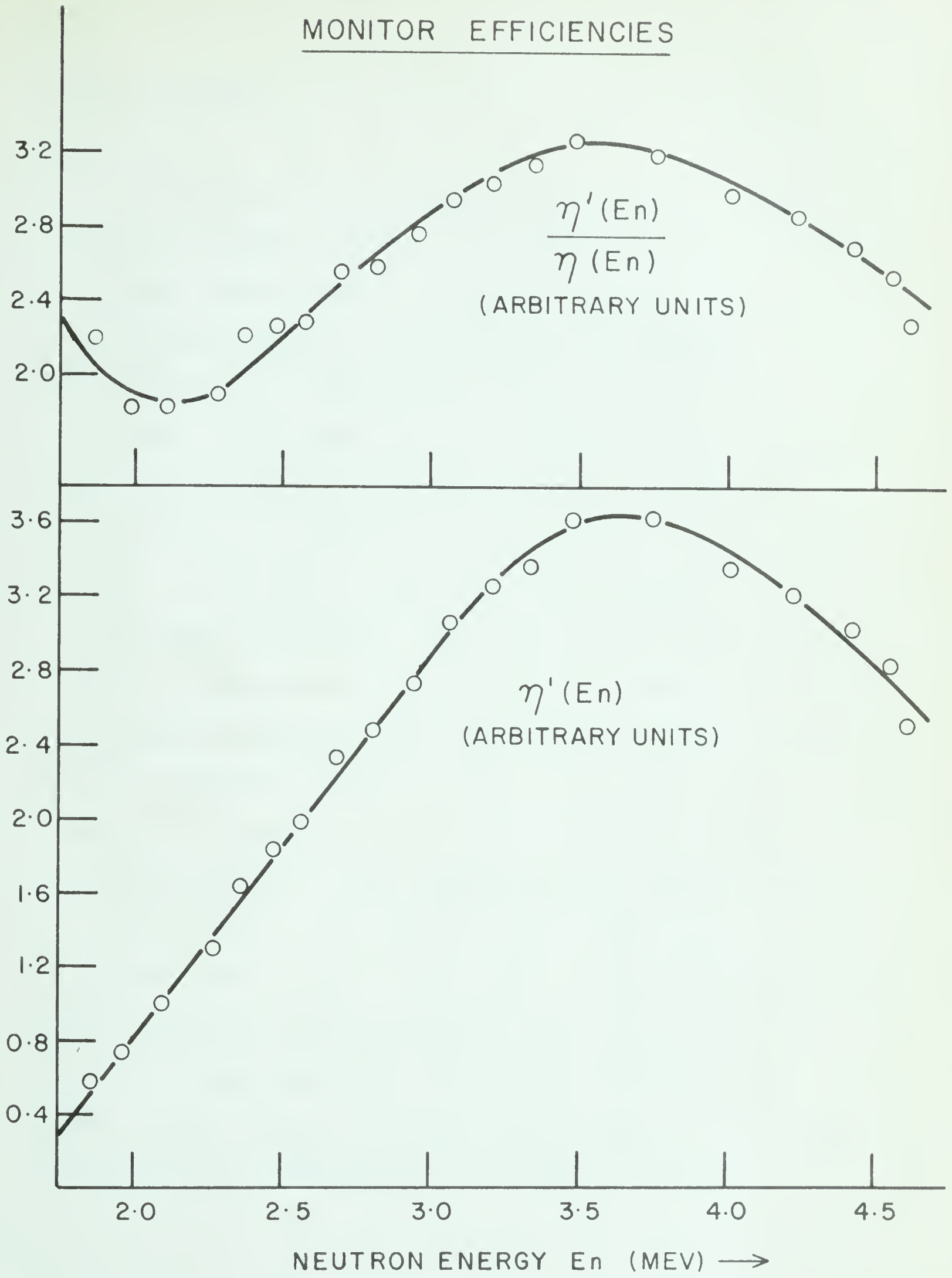
MONITOR EFFICIENCIES
3·2
2·8
2·4
2·0
η'(En) / η(En)
(ARBITRARY UNITS)
3·6
3·2
2·8
2·4
2·0
1·6
1·2
0·8
0·4
η'(En)
(ARBITRARY UNITS)
2·0
2·5
3·0
3·5
4·0
4·5
NEUTRON ENERGY En (MEV) ⟶

FIG. I—4

about 4.5 MeV.

One expects the efficiency to fall off at higher energies because of the n-p cross-section. The additional decrease observed can be explained when one looks at the raw data pertaining to the efficiency experiment. The total counts, as measured by the emitter follower connected to the tenth dynode, seem to follow roughly, when divided by the n-p cross-section, the differential cross-section for neutrons given by Brolley and Fowler (Br60). The monitor counts fall off at small angles (high energy neutrons). The total count rate at small angles is approximately three thousand counts per second. A possible explanation for this effect is pulse pile-up in the amplifying stages, some of which are direct-coupled. A change in the DC level could shift the operating points of the transistors and cause blocking or reduced gain. As a result, the trigger circuit would register fewer counts. Gain shift in the photomultiplier with increased count rate could also be a factor. It was unfortunate that the monitor was not tested at a much larger distance from the target, say 1 - 2 meters. Ultimately, the monitor will be placed at such a

distance when in service.

It is also useful in neutron dosimetry to define the efficiency in another way. The efficiency at energy E is usually defined as the number of counts (per second) from the monitor, divided by the number of neutrons incident per square centimeter (per second) at energy E (Vr61). The incident flux is usually measured by some standard counter, like a BF_3 long counter. For the present monitor, one obtains the figure 2.5 counts per neutron/cm^2, for a neutron energy of 2.8 MeV. De Vries and Udo obtained a mean efficiency of 0.9 counts per neutron/cm^2 for a Po-Be source, using a stilbene crystal and a slightly different circuit.

Some difficulty was encountered in adjusting the parameters of the circuit for optimum gamma discrimination. Brooks (Br59) describes a "twinckle box" by means of which the separation of proton and electron pulses is displayed on an oscilloscope screen. Such a device would have been convenient for adjustment purposes, as well as for giving an indication of the minimum energy protons passed by the gamma discrimination circuit.

Apart from the characteristics of the electronics used to provide separation of the proton and electron pulses, the discrimination process is governed by another factor; statistics. For the average scintillation in a liquid or plastic phosphor, it requires approximately 1.4 keV of energy dissipated in the crystal to produce one photoelectron at the photocathode. When one considers that the slow component contains about 20 percent of the total current in a scintillation, the information delivered to the pulse-shape discriminator is carried initially by less than 300 electrons for a proton pulse of 2 MeV. Statistical fluctuations in this number and, of course, the inherent fluctuations in phototube gain, make the pulse-shape discrimination process very much subject to uncertainties. This is why the circuit used should be designed to take maximum advantage of the discrimnation properties of the scintillator. Gatti (Ga61) describes a filter which he constructed for use with an anthracene crystal. He was able to discriminate against all electrons whose energy was less than 39 keV. His circuit and the one due to Alexander and Goulding (Al61) use essentially the same principle; the pulse is integrated and then differentiated twice. This process enhances

the difference between slow and fast components. The two circuits perform these operations in different order, however, but similar results are obtained.

6. Conclusions -

The response of the fast neutron monitor is sufficiently good over the energy range of neutrons available in this laboratory. The transistor circuits are quite reliable, and the device should require very little maintenance. Photomultiplier voltage is not critical, but reduced separation of the fast and slow components occurs for voltages greater than about 1750 v. The transistors will run on any voltage from 20 - 30 v. No additional adjustments are necessary.

II. THE SEMICONDUCTOR JUNCTION DETECTOR APPLIED TO SOME ALPHA PARTICLE REACTIONS.

1. Introduction

Within the last five years, a new detector of charged particles has become available to physicists. It is the semiconductor junction detector, sometimes referred to as the solid state ionization chamber. It is small in size, requires no high voltages, and has an extremely fast response. The output is proportional to energy, and particle groups separated by as little as 30 keV can be resolved. In addition, the solid state detector is insensitive to neutrons and gamma rays to a very high degree. It thus makes an extremely versatile charged particle spectrometer.

There are large areas of particle research which are particularly well suited for investigation using semiconductor detectors. These include studies of charged particles in coincidence with neutrons and gamma rays, angular distributions, and excitation functions.

It was decided to set up a system at the University of Alberta Van de Graaff Laboratory whereby the angular distributions of charged reaction products could be observed, as well as particle spectra from different reactions.

2. Beam Hardware

The 2 MeV Van de Graaff generator accelerates protons or deuterons. The experimental arrangement for the present work is indicated in figure II-1.

Beam energy is set by the magnet and regulated by corona stabilization of the accelerating voltage. This stabilization is accomplished using an error signal from the vertical pair of beam defining plates. Both the vertical and horizontal plates are made of 0.010" tantalum, and can be moved in and out by means of micrometer dials. At this point the beam can be brought to any desired rectangular shape, to an accuracy of 0.001" in either direction. A quartz viewer follows, so that the beam size and focus may be observed.

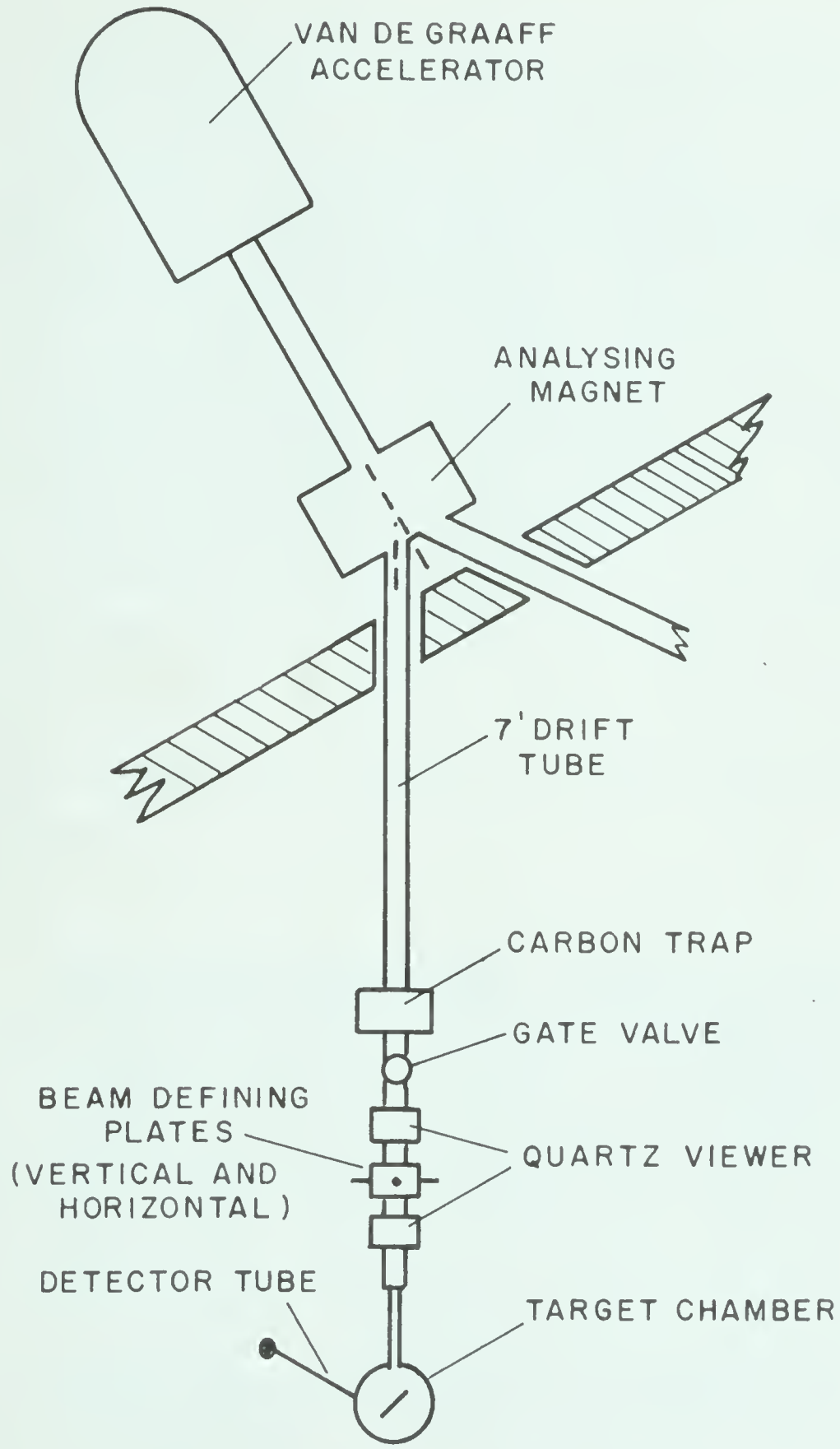

EXPERIMENTAL ARRANGEMENT

FIG. II – 1

The detector is attached to a sliding vacuum seal on the target chamber. Reaction products can be observed in the angular range of -140° to $+120^{\circ}$ with respect to the incident beam direction. Target-to-detector distance can be varied from 1 3/4" to 5". The insulated target holder can be raised, lowered, moved sideways, and rotated about a vertical axis. When using a target with a thick backing, the positive terminal of a 45 v battery is connected directly to the target. The negative terminal is then connected, by means of a shielded cable, to a Model A309A Current Indicator and Integrator*. For thin target work, a Faraday cup inside the chamber is used to collect the beam. It is connected electrically to the target, and the battery and integrator are used as before.

The target chamber also contains a thin Am^{241} alpha source used for detector resolution measurements, and a small slab of quartz for checking the beam alignment. Both the source and the quartz are swung out of the way when not in use.

*Elcor Inc., Falls Church, Virginia, U. S. A.

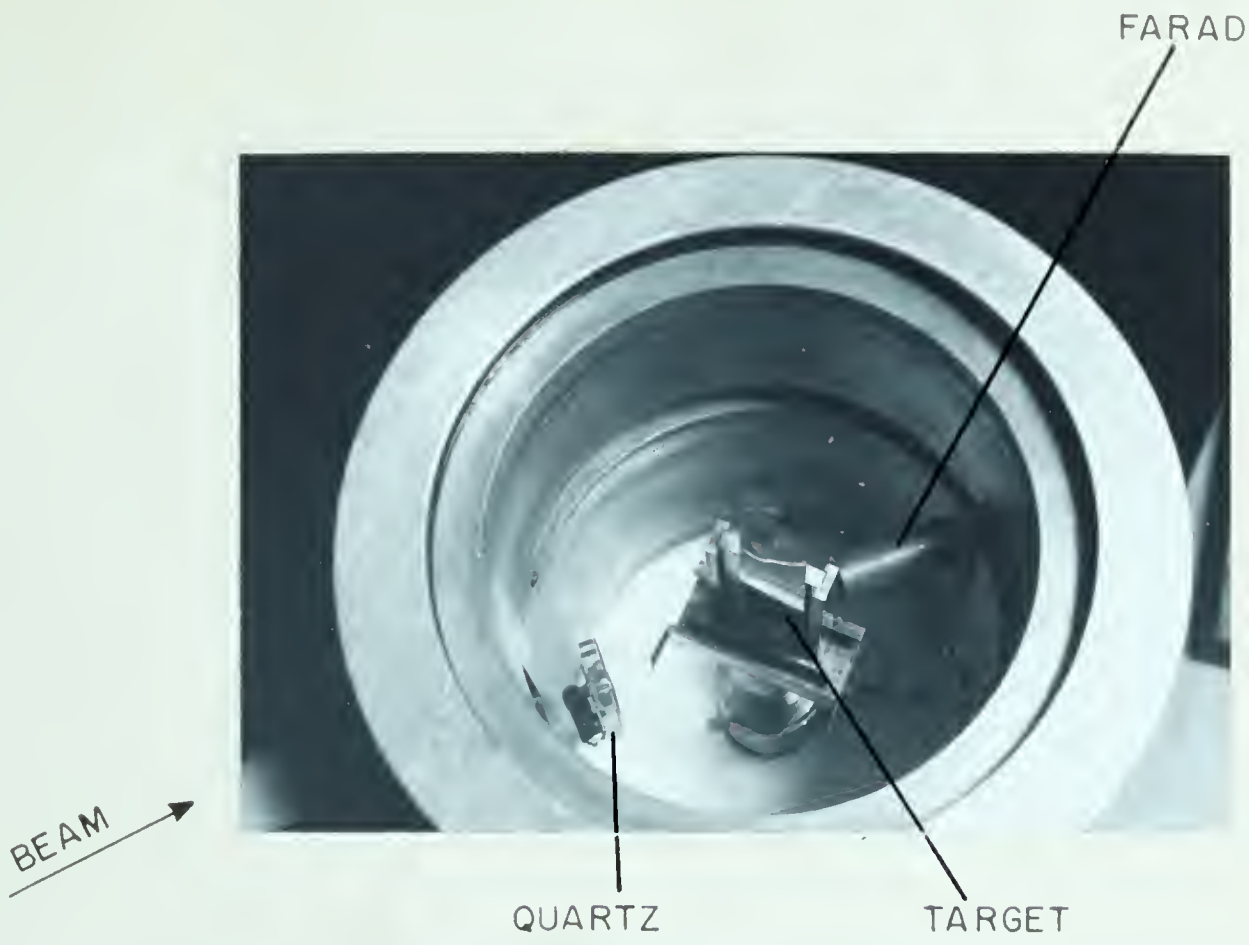

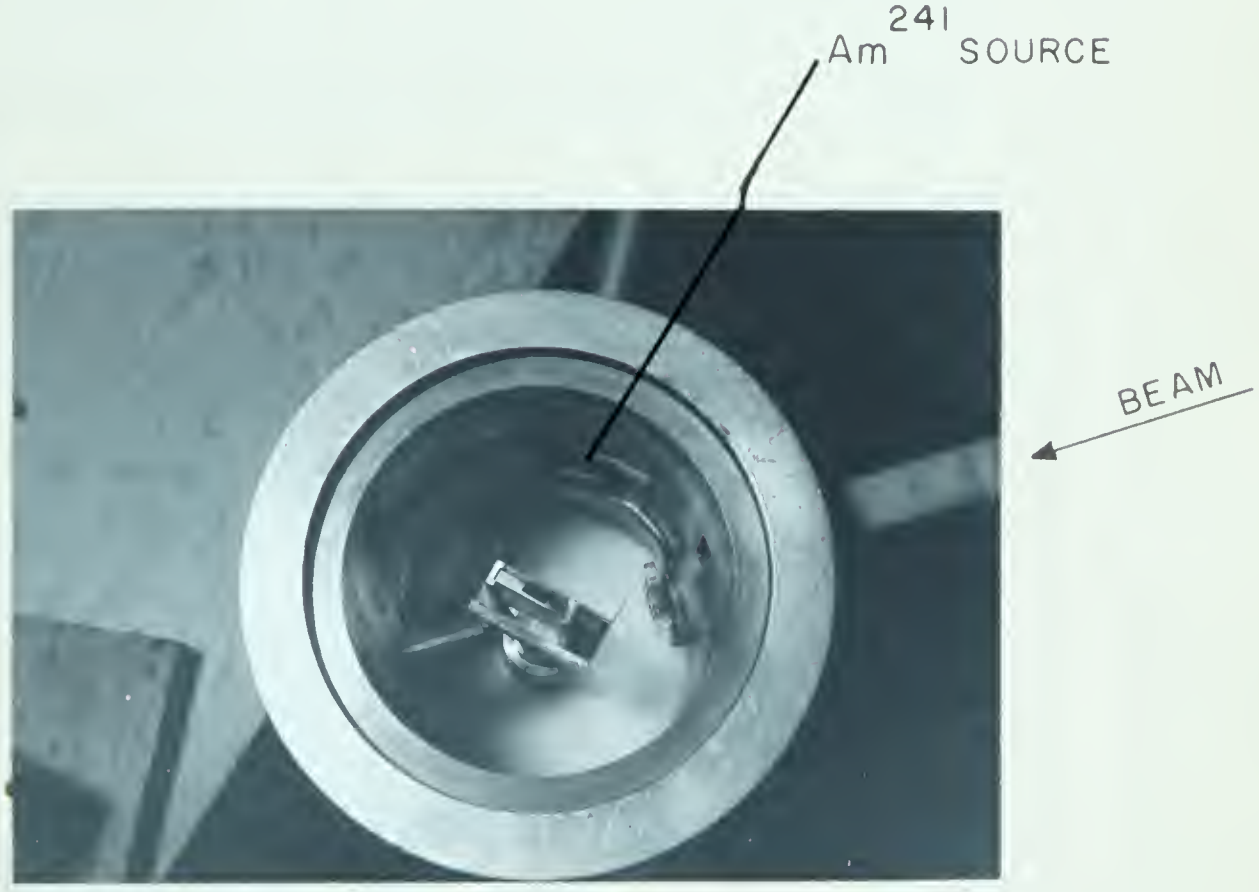

TARGET CHAMBER

GAMMA MONITOR

TARGET CHAMBER

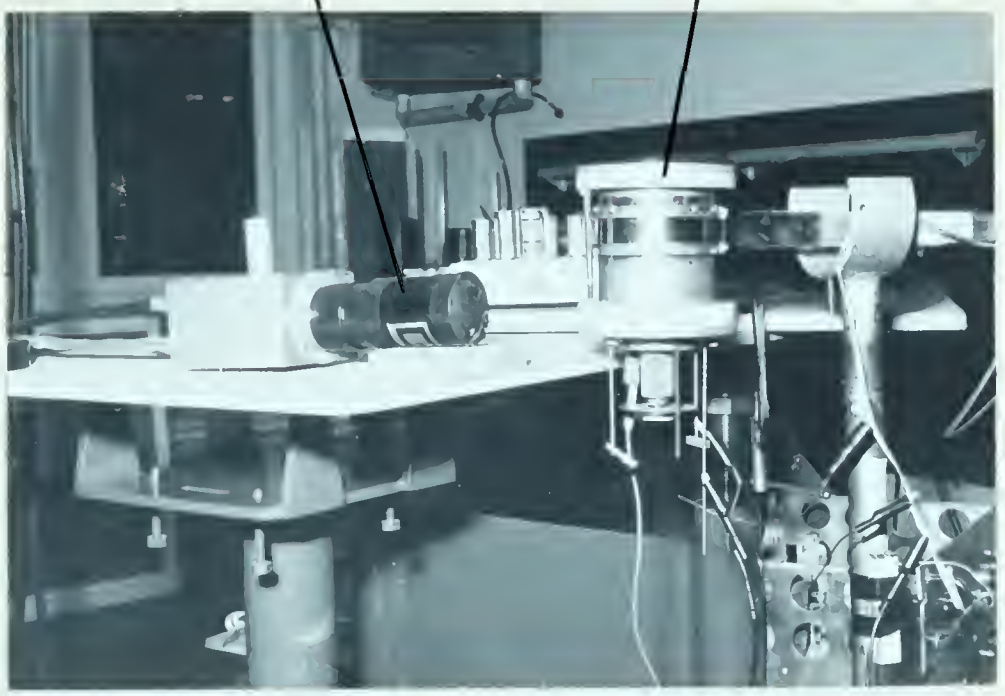

DETECTOR TUBE

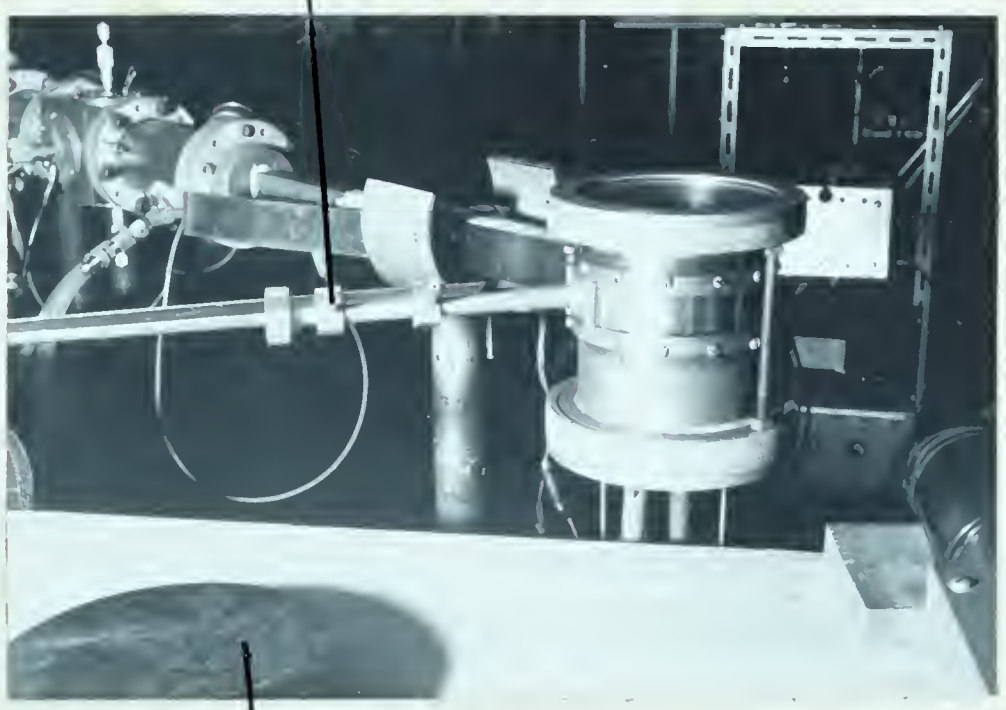

LIGHT CAP

BEAM
VIEWERS

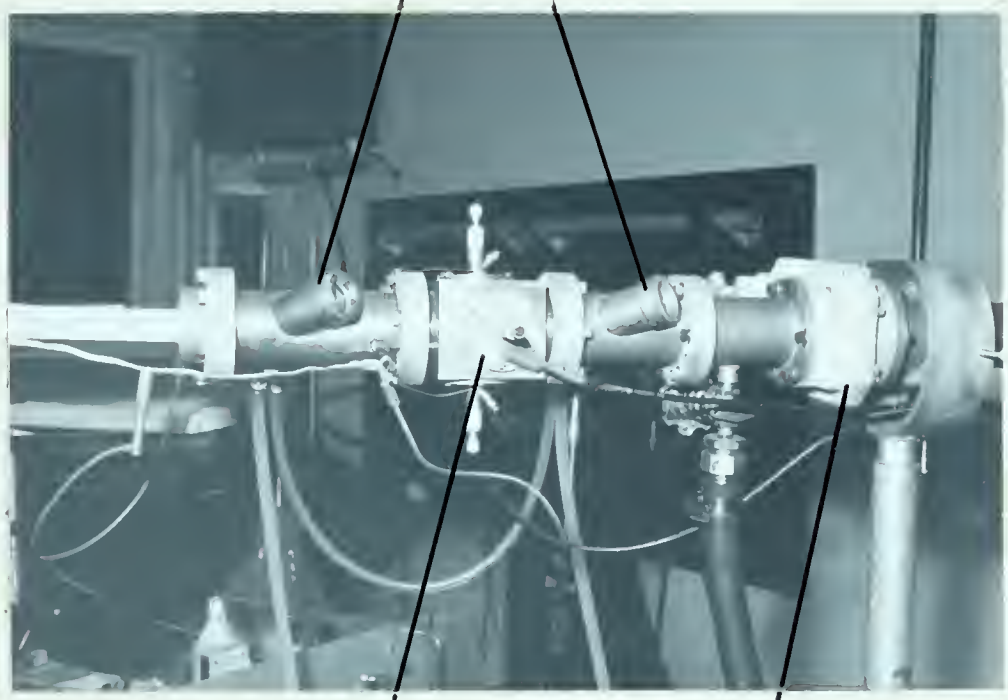

BEAM DEFINING
PLATES

GATE VALVE

3. Operation of the Semiconductor Junction Detector

(a) Physical Processes

The diffused junction semiconductor detector operates on the same principle as a gaseous ionization chamber, except that the sensitive volume is a crystal lattice. Charged particles entering a region of high electric field produce hole-electron pairs by collisions in the lattice. These pairs drift under the action of the field to opposite sides of the sensitive volume, and constitute a flow of charge which can be observed. The high field region, known as the depletion region, is formed in the following manner. Electron donor impurities (eg. phosphorus) are diffused in a very shallow layer on to the surface of a small slab of high purity p-type silicon. This surface layer is thus n-type, with a high concentration of electrons. The main body, being nearly intrinsic material, has a low concentration of holes, and is p-type. Electrons from the n-layer tend to diffuse to the p-region, and holes from the p-region tend to diffuse to the n-layer. The result is the erection of a potential barrier at the junction of the two regions

which impedes the flow of charge at equilibrium. The magnitude of this barrier is typically 0.5 v . The space charge region so formed must contain an equal number of positively charged donor atoms and negatively charged acceptor atoms. The acceptor concentration is low because the p-type silicon is of a high purity. As a result, the space charge, or depletion layer extends almost entirely into the p-type material. Under these conditions the depletion depth can be of the order of 10^{-3} cm.

Another type of detector, known as the surface barrier, is made by thoroughly cleaning and polishing the surface of a slab of n-type silicon. A p-type layer forms spontaneously on the surface, and electrical connection is made by evaporating on a thin gold film. The principle of operation is the same as in the diffused junction detector.

The detector is depicted schematically in Figure II-2, along with the corresponding charge distribution. To obtain the potential distribution, we solve

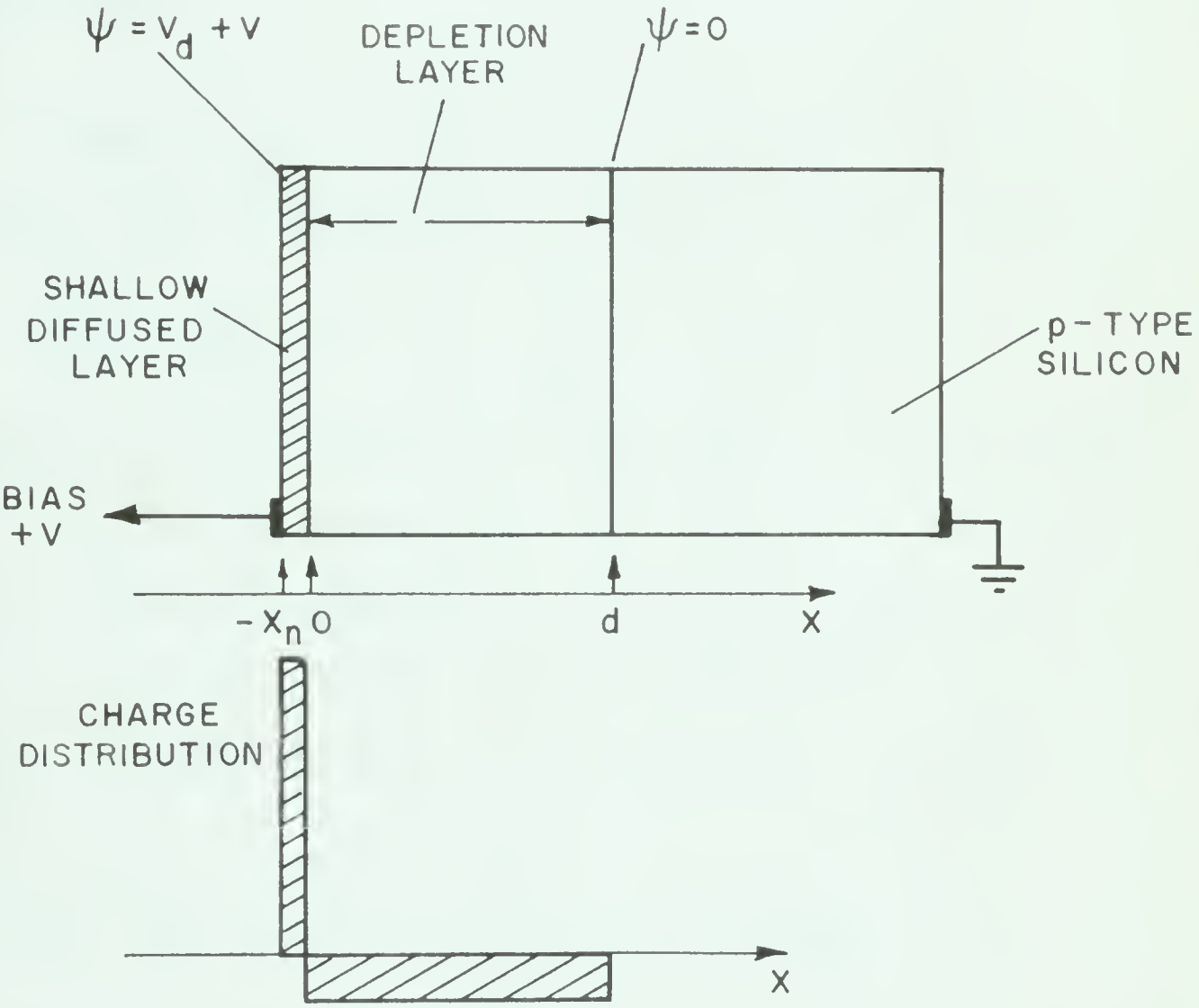
ψ = V_d + V
DEPLETION LAYER
ψ = 0
SHALLOW DIFFUSED LAYER
p - TYPE SILICON
BIAS +V
-x_n 0
d
x
CHARGE DISTRIBUTION
x

FIG. II - 2

Poisson's equation*. The charge distributions, denoted by ρ, may be approximated by constants. Actually, ρ varies with x in the n-layer because the diffusion is not uniform with depth, but in practice this layer is 1/1000 as thick as the p-layer. so any variations are negligible.

Treating the n-layer as the left side, and the p-layer as the right side, we have for the potential ψ

$$\frac{\partial^2\psi}{\partial x^2} = \frac{-\rho}{\epsilon\epsilon_o} \quad ; \qquad \begin{array}{ll} \rho = qN_d & -x_n \leqslant x \leqslant 0 \\ \rho = -qN_a & 0 \leqslant x \leqslant d \end{array} \qquad (1)$$

where N_d is the density of donor atoms in the n-layer

N_a is the density of acceptors in the p-layer

ϵ is the permittivity of silicon (about 11)

ϵ_o is the permittivity of free space

and q is the charge of the electrons and holes.

The boundary conditions are : $\psi_L = V_d + V$ at $x = -x_n$, the depth of the diffusion layer, $\frac{\partial\psi_L}{\partial x} = 0$ at $x = -x_n$; $\psi_R = 0$ at $x = d$, the depth of the

*This treatment is similar to that given in To61.

depletion region, $\frac{\partial \psi_R}{\partial x} = 0$ at $x = d$. V is an external bias voltage, and V_d is the potential barrier mentioned above. Solving for the potentials and the fields we obtain

$$\psi_L = V + V_d - \frac{qN_d}{2\epsilon\epsilon_o} (x + x_n)^2$$

$$E_L = \frac{qN_d}{\epsilon\epsilon_o} (x + x_n)$$

$$\psi_R = \frac{qN_a}{2\epsilon\epsilon_o} (d - x)^2 \qquad (2)$$

$$E_R = \frac{qN_a}{\epsilon\epsilon_o} (d - x)$$

Equating fields and potentials at $x = 0$, and remembering that $N_d >> N_a$ because of the purity of the p-region, we obtain the following expression for the depletion depth d:

$$d = \sqrt{\frac{2(V + V_d)\epsilon\epsilon_o}{qN_a}} \quad . \qquad (3)$$

From a well-known relation of solid state physics (De60),

$$N_a = \frac{1}{\rho q \mu_h} \quad , \qquad (4)$$

where ρ is the resistivity of silicon

and μ_h is the mobility of holes in silicon.

Therefore

$$d = \sqrt{2(V + V_d)\rho\mu_h c\epsilon_o} \quad . \tag{5}$$

To find the capacity per unit area of the diode, we take $C = \frac{dQ}{dV} = \frac{d}{dV}(N_a q d)$. (6)

$= \frac{\epsilon\epsilon_o}{d}$, which is the same expression obtained for a parallel-plate capacitor. The dependence of the capacity on the applied voltage is

$$C = \sqrt{\frac{\epsilon\epsilon_o}{2(V + V_d)\mu_h\rho}} \quad . \tag{7}$$

From the above considerations, we note that both the capacity and the depth of the depletion region are dependent upon an externally applied reverse bias, and the resistivity of the material. It is found that those particles energetic enough to pass right through the depletion region produce a non-linear response from the diode, while those that are completely stopped in the active region produce an output exactly proportional to their energy. This is true independent of the mass or charge of the incident particle. The semiconductor detector responds only to the energy of the incident particle. In the devices available commercially at the

present time, depletion layers can be formed equivalent to the range of 10 MeV protons, and thus these detectors are ideal for use in obtaining energy spectra from nuclear reactions.

(b) Collection Time of Charges

The creation of the hole-electron pairs is an extremely rapid process, and is expected to be much faster than the diffusion times of the carriers across the depletion layer. Assuming all the pairs to be created at time t = 0, the collection time of the charges may be simply estimated by dividing the depletion region depth by the average velocity. Considering the holes (the result is identical for electrons*), we have

$$t_h \sim \frac{d}{\bar{v}} \sim \frac{d}{1/2\mu_h E_{max}} = \frac{d}{1/2\mu_h \left(\frac{V_d + V}{d}\right)}$$

$$= \frac{2d^2}{\mu_h (V_d + V)} = \frac{4(V_d + V)\rho\mu_h \epsilon\epsilon_o}{\mu_h (V_d + V)}$$

$$= 4\rho\epsilon\epsilon_o \quad . \tag{8}$$

This calculated collection time is independent of the bias voltage applied. For 1000 ohm-cm silicon the charge is collected in about 5 nsec. Of course this

*up to a constant $\frac{\mu_h}{\mu_e} = 0.33$

treatment is valid only for the pairs created in the depletion layer. If the particle penetrates beyond, there will be an additional slow component due to the diffusion time of the carriers in the field-free region.

Experimentally, however, it is found that additional factors, like the bias voltage, do affect the rise time of the output pulse. The intrinsic base resistance of the material behind the depletion region may be in some way responsible for the lengthened rise times experimentally observed (De61, Ra61). Extremely fast response detectors can be constructed by extending the depletion region to the back of the detector. The rise-times observed approach the theoretical values, being in the nanosecond range.

(c) Output

The detector is essentially a capacitor upon whose plates a voltage is induced by the collection of the holes and electrons. The magnitude of this voltage pulse is dependent upon the capacity, and thus on the bias, going as $(V)^{1/2}$. If the voltage output mode is

used, great care must be taken to keep the external shunt capacitance to a minimum, since excessive capacitance reduces the signal-to-noise ratio for succeeding stages.

A more suitable way of obtaining the output signal is by using a charge-sensitive amplifier. Here the AC voltage across the detector is made zero by the use of feedback, and the charge flows into a condenser of fixed value across which an integrated voltage appears. The signal-to-noise ratio is not improved by this method, but fluctuations due to changes in detector capacity are eliminated. Of course, a low noise preamplifier is essential in both voltage- and charge-sensitive applications. Circuits for this purpose have been designed and are available commercially.

(d) Noise

The main source of noise in the semiconductor junction detector is the reverse leakage current. Such a current is expected since the device is a p-n junction diode operating under reverse bias. Like the diffusion depth, the leakage current has been found to increase

as $(V)^{1/2}$ (De61), indicating that leakage current noise is to a large extent governed by the space charge. Recombination centers in the space charge region generate holes and electrons, and the number of such centers increases with the depletion depth. This effect limits the bias voltage which can be applied. Additional noise is caused by fluctuating conditions at the edge of the junction, giving rise to a surface leakage current. It has been found that cooling the detector reduces the leakage and increases the breakdown voltage (Bl61). In this way much higher bias voltages may be applied.

Light incident upon the face of the detector is another source of noise. The energy gap in silicon (the energy difference between the bottom of the conduction band and the top of the valence band) is 1.21 eV, which corresponds to a wavelength of 10,000 Å. Under exposure to light, holes associated with the acceptors of the p-type silicon may be excited into the conduction band, causing a leakage current to flow. This random process is a prolific source of noise; measurements in this laboratory indicate the RMS noise voltage of a detector decreases by as much as 25% when

operated in the dark.

Particles incident on the front face of the detector are required to pass through the thin diffusion or "dead" layer. This introduces a window effect, also noticed in gaseous ionization chambers. In the RCA detectors used in this laboratory*, dead layers of 2 and 0.2 microns are present on the detectors. This corresponds to a thickness of 0.48 and 0.05 mg/cm^2 of silicon respectively. In the former case, the correction to alpha particle energy amounts to 250 kev at 5.5 MeV, so care must be exercised when using these detectors for absolute energy calibrations. For the thinner diffused detectors, the correction is reduced by a factor of ten.

Resolution measurements have been made by many different groups on detectors both commercially available and fabricated in their laboratories. The resolution is defined as the full width at half maximum of the peak due to a monoenergetic particle group, divided

*RCA Victor Co. Ltd., Electron Tube and Semiconductor Division, Montreal, P.Q.

by the energy of the group. Up to the present time the lowest energy spread observed has been 15 keV (B160), with a silicon-gold surface barrier detector. This corresponds to a resolution of 0.27%. 26 keV has been realized in this laboratory, using a thin Am^{241} source, an RCA type A-4-75-0.2 detector, and the Ortec Model 101-201 Amplifier-Preamplifier* (see figure II-3).

Statistical fluctuations play a much smaller part in determining the resolution of a semiconductor detector than in scintillation and gas proportional counters. This is due to the lower energy requirements for producing the charge carriers. Recent work (Ba60) gives the figure of 3.23 $\pm$.04 eV required to produce one hole-electron pair in silicon. Ten times as much energy is needed to produce an ion pair in a gas counter, whereas the corresponding figure for the scintillation counter is 700-1200 eV per photoelectron. For a 5 MeV alpha particle, approximately 15 million hole-electron pairs are produced within the sensitive volume of the semiconductor detector. Recombination of

*Oak Ridge Technical Enterprises Corp., Oak Ridge, Tenn., U. S. A.

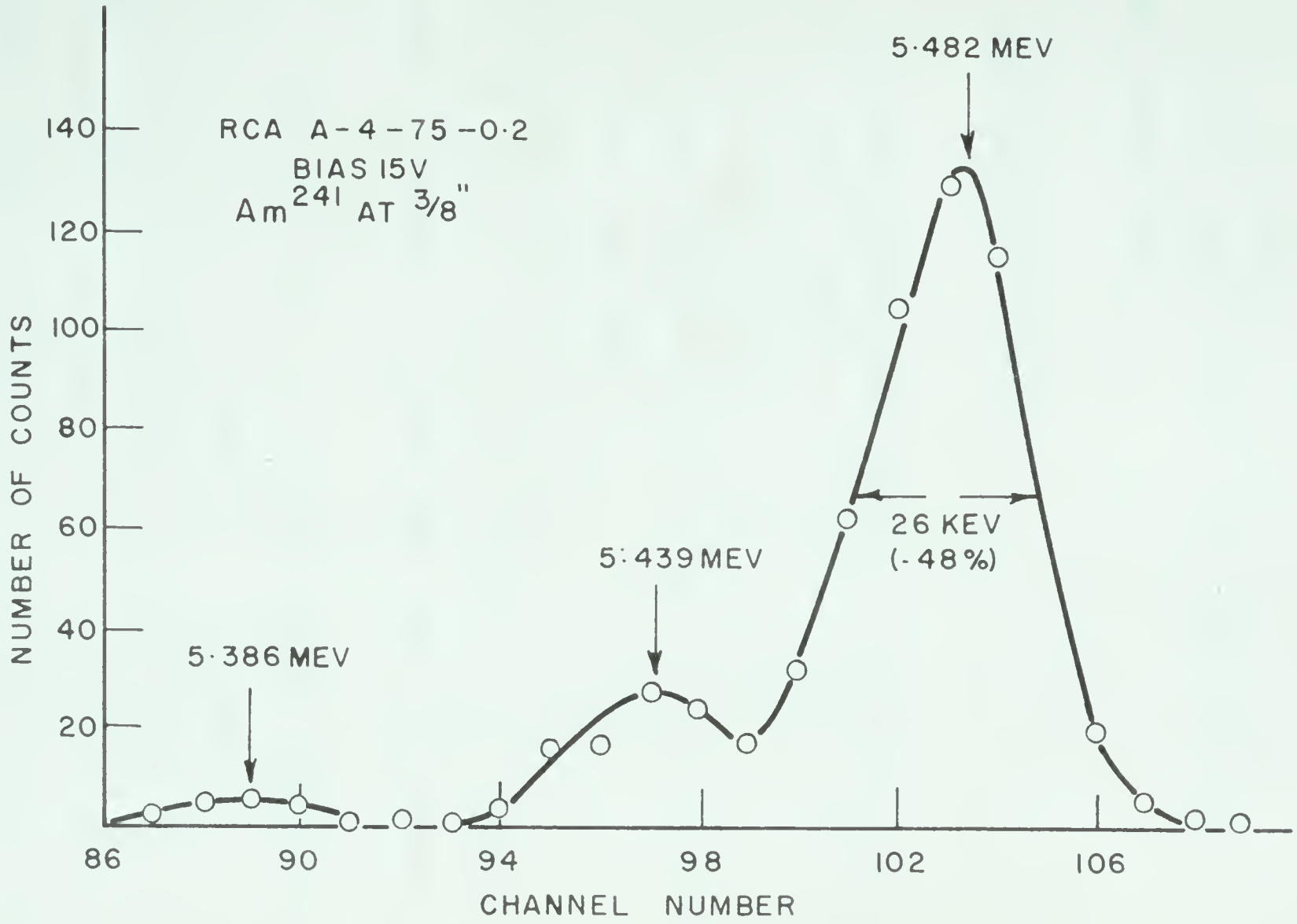

TYPICAL DETECTOR RESOLUTION MEASUREMENT

FIG. II – 3

holes and electrons can reduce this number, and trapping centers present in the crystal lattice can spread the charge collection time into the microsecond range. These effects can be reduced by careful control of impurities in the crystal, and by keeping the depletion depth less than about 10 mm (Br61).

4. Experimental Results

In the present experimental arrangement, the small size of the target chamber necessarily exposes the detector to a high flux of charged particles. Such a flux consists not only of the reaction products, but of an even larger number of scattered beam particles. The purpose of the first experiment was therefore to determine the effect of a high charged particle flux on the energy response of a detector. No attempt was made to measure any rise time changes.

Following this, it was decided to observe some alpha particle angular distributions. For the first measurement, the ground state alpha particles (α_o) from the reaction $F^{19}(p,\alpha)O^{16}$ were chosen. They have the advantage of high energy, large separation from the other alpha groups, and

moderate yield.

The angular distribution was then observed for the well-known α_1 group leading to the 6.135 MeV level in O^{16}. This group is separated in energy from the bombarding protons by only 1.5 MeV. Any faults in the instrumentation due to excessive count rate would show up under these conditions, and could then be corrected.

Finally, the charged particle spectrum was observed from the bombardment of B^{11} by deuterons. This is of interest because of the neutron time-of-flight experiments being conducted in this laboratory on the reaction $B^{11}(d,n)C^{12}$.

(a) Behaviour Under Excessive Bombardment

Various authors have discussed the effect of high neutron and gamma ray backgrounds on solid state detectors (Kl61, Ma62). However, little mention has been made of the effects of charged particle fluxes. Because of present and potential applications of solid state detectors in this laboratory, an attempt was made to study the resolution of a detector as a function of total integrated counts. The

detector used was an RCA type A-3-25-2.0, resistivity $10^3 \Omega$-cm, area 5 mm^2. For this experiment, 1 MeV protons were scattered into the detector from a gold foil of thickness 170 $\mu g/cm^2$. With a beam current of about 0.04 μa, the count rate at the detector was approximately 15,000 protons/sec. Resolution tests with the Am^{241} source were taken before the experiment and after total integrated counts of 10^7, $5x10^7$, 10^8, $1.5x10^8$, $2x10^8$, $2.5x10^8$, $3x10^8$, $3.5x10^8$, $4x10^8$, $5x10^8$, $6x10^8$, and $7x10^8$. The results are summarized below and in Figures II-4 & 5. The initial resolution was 1%. After the first bombardment, the resolution improved slightly to .82%. After $5x10^7$ counts, a subsidiary peak appeared on the low energy side, and the whole peak was spread out. When 10^8 total counts had been absorbed, the low energy peak had disappeared, and the resolution was approximately 1.4%. After $1.5x10^8$ counts, the peak was badly smeared out, with a resolution of 2.7%. $2x10^8$ counts produced a subsidiary peak on the high energy side, with the main peak half-width being 196 keV (3.6%). The worst spectrum occurred after $2.5x10^8$ counts. The subsidiary high-energy peak was only slightly evident, and the width of the peak corresponded to a resolution of 4.7%. An abrupt change was noted after $3x10^8$ counts. The resolution

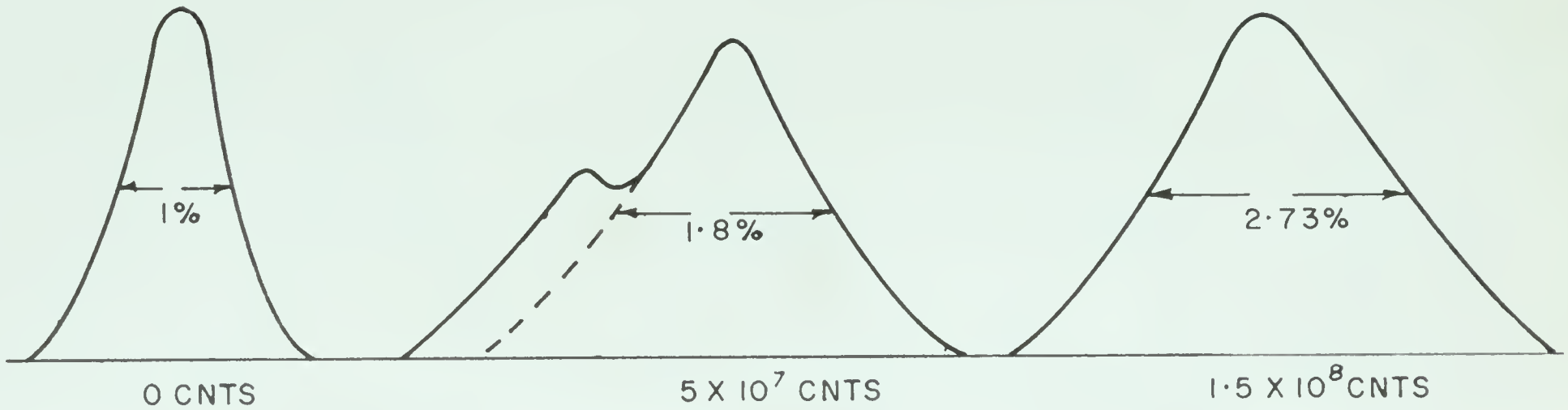

Am^{241} SPECTRA AFTER PROTON BOMBARDMENT OF DETECTOR

FIG. II - 4

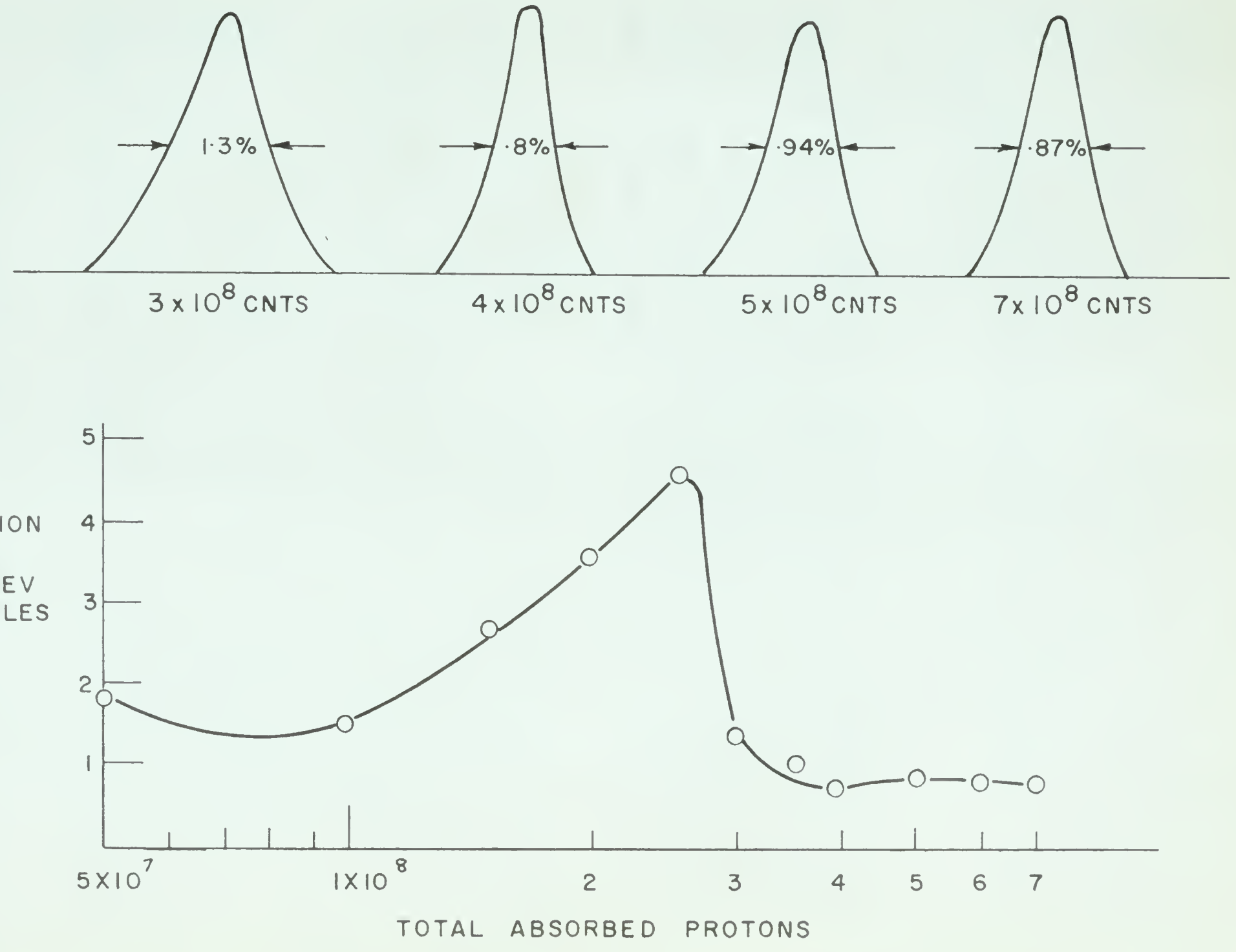
1·3%
·8%
·94%
·87%
3 x 10^8 CNTS
4 x 10^8 CNTS
5 x 10^8 CNTS
7 x 10^8 CNTS
RESOLUTION (%) FOR 5·482 MEV α PARTICLES
5
4
3
2
1
5X10^7
1X10^8
2
3
4
5
6
7
TOTAL ABSORBED PROTONS

FIG. II - 5

dropped to 1.3%. Further bombardment only served to improve the detector's resolution, with the final value of 0.87% being achieved after 7×10^8 counts. During the experiment the energy peak shifted only one or two channels. Bias voltage was 15 v.

Other workers have reported that no changes in detector operation were observed after bombardment by 10^{12} 14 MeV protons (Fr61). However, Dearnaley and Whitehead (De61) found their surface barrier detectors deteriorating after absorbing approximately 10^7 5.5 MeV alpha particles.

It is difficult to offer an explanation of the effect observed on the present detector, since a sample of one tells nothing about the general population. However, the heavy bombardment may have been enough to heal some imperfection in the crystal lattice, or to alleviate a surface contamination. Every precaution was taken to assure that the deviations were not being caused by instrumental effects. The Ortec amplifier system and the 256-channel TMC pulse-height analyser* were tested in conjunction for stability

*Technical Measurements Corp., North Haven, Conn. U.S.A.

over a 12-hour period, and the observed drift was less than two channels. For this experiment the two were allowed to warm up at least an hour before the measurements were taken. The resolution of the detector was measured again six weeks after the experiment, with no change from the previous measurement. This indicated that the observed improvement was not a transitory effect. However, it does appear that excessive charged particle bombardment has no detrimental effect on the detectors as far as their energy response is concerned.

(b) $F^{19}(p,\alpha_o)O^{16}$

The excitation function of this reaction has a resonance at a proton bombarding energy of 843 keV. Since the energy of the ground state alpha particles varies from 6.8 to 7.6 MeV in the angular range studied, an aluminum absorber of thickness 3.3 mg/cm^2 was interposed between the target and detector. This thickness is equivalent to the range of 1 MeV protons and 3.5 MeV alpha particles. Consequently, all scattered protons and lower energy alpha particles were unable to reach the detector, and the results obtained were free from background.

The target was made by evaporating a thin layer of CaF_2 onto a 0.56 mg/cm^2 nickel foil. Since this foil had a thickness of only 76 keV for 0.84 MeV protons, the Faraday cup was used to collect the beam. The target thickness was measured to be 9 keV at 873 keV. This was accomplished by observing the variation in yield of 6-7 MeV gamma rays in the vicinity of the $(p,\alpha\gamma)$ resonance in fluorine at 873.5 keV. The accelerator voltage scale was also calibrated using this resonance.

For this work, the bombarding energy was set at 853 keV, where maximum alpha particle yield was obtained (the target was $\sqrt{2}$ thicker because of its orientation; see below). Beam current was 0.08 μa. During the experiment the energy of the accelerator was constant to within 0.25%.

The target was placed with its outward normal at an angle of -135° to the incident beam direction. An angular range of from -65° to -140° was covered by the detector, and it subtended a solid angle of 1.9×10^{-3} sr. Forward angle measurements were also attempted, with the target turned so that its outward normal made an angle of +135 with the beam. In this position the alpha particles had to pass

through the nickel backing on their way to the detector, suffering an energy loss of just under 200 keV. This thickness caused some loss of yield by coulomb scattering, so the raw data was normalized to the back angle values using three common points. Angles from -30° to -90° were covered, the Faraday cup interfering with angles between -30° and 0°.

Angular distribution data measured in this way must be converted from laboratory coordinates to center-of-mass coordinates, the correction involving a change in the angle and in the yield per unit solid angle. Convenient tables are available for performing this conversion (Ma54). The final results are plotted in Figure II-6, together with points obtained by Isoya et al (Is58) and Rubin (Ru47). There seems to be disagreement for $\cos\theta_c > 0.5$, with Rubin's yield decreasing, and Isoya's increasing.

On the basis of his results, Isoya assigns a J^{π} value of 2^{+} to the 13.674 MeV level in Ne^{20} involved with the 843 keV resonance for the ground state alpha particles (Is58a). Since both the alpha particle and the ground state

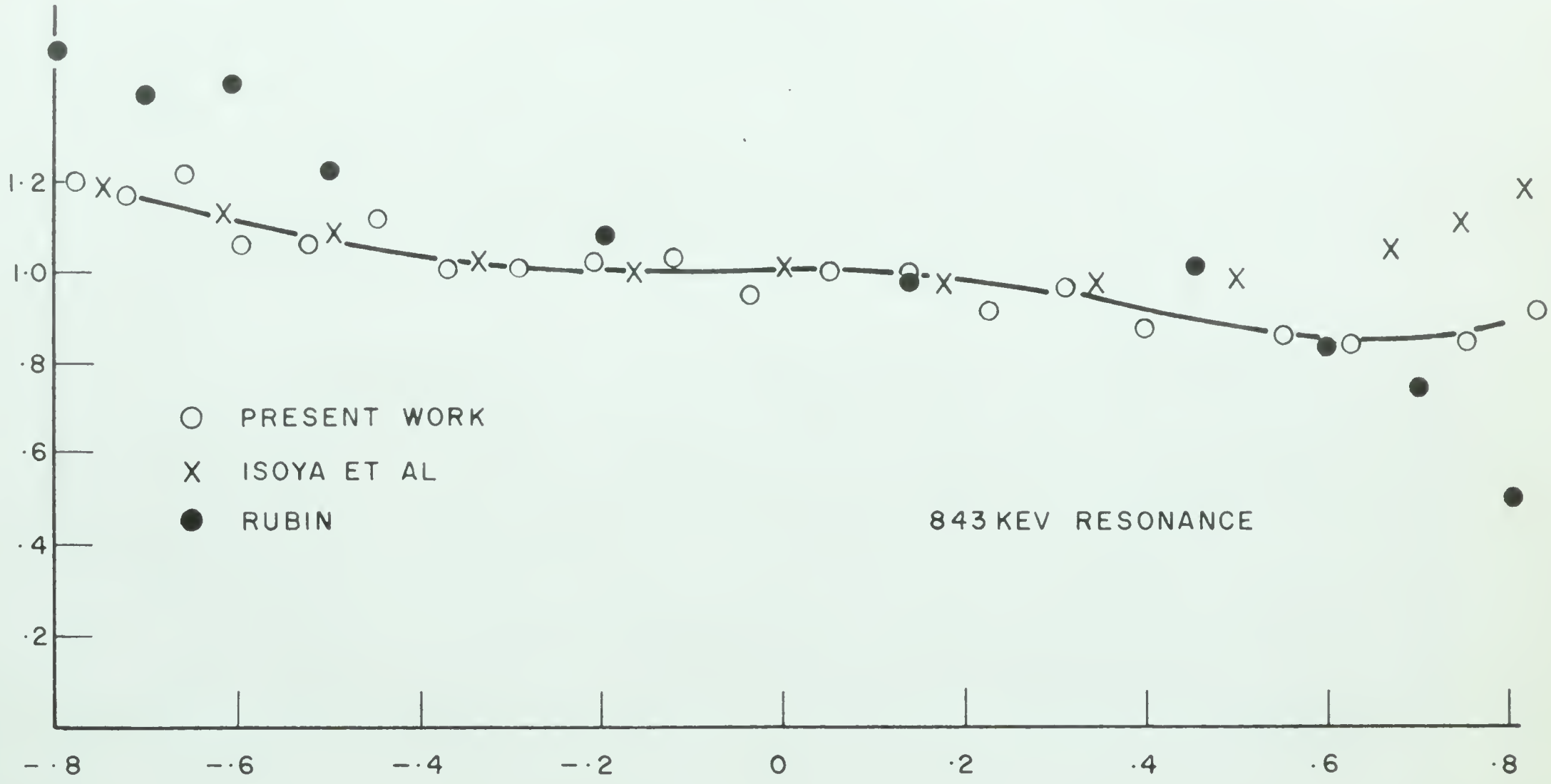

ANGULAR DISTRIBUTION OF $F^{19}(p, \alpha_0) O^{16}$

FIG. II - 6

of O^{16} have zero spin and even parity, only states of the compound nucleus Ne^{20} which have even spin and even parity or odd spin and odd parity can decay by α_o emission. In addition, the angular momentum of the emitted alpha particle will be equal to the spin of the compound level. An assignment of 0^+ to such a level in Ne^{20} would require an isotropic distribution of the emerging alpha particles. An assignment of 2^+ would cause the distribution to contain terms in Legendre polynomials P_o, P_2, and P_4 if the resonance were not subject to interference from neighboring states. Very few of the distributions measured at various bombarding energies by Isoya et al (Is58) are symmetric about 90^o in the center-of-mass-system, indicating that there are broad resonances in the compound system whose effects extend to other states.

It should be noted that Baranger (Ba55) has assigned the spin and parity of this state as 0^+ on the basis of results from $F^{19}(p,p')F^{19}*$.

(c) $F^{19}(p,\alpha_1)O^{16}*$

The study of this alpha group is considerably simplified by the fact that the excited O^{16} nucleus decays immediately

by gamma emission. The resonance, in this case the prominent one at E_p = 873 keV, can be determined precisely with the help of a scintillation counter. In addition, deterioration of the target or energy shifts off resonance can be immediately discovered if the gamma yield is monitored continuously, as it was in this experiment. However, the alpha group is of low energy, ranging from 2.0 to 2.4 MeV in the angular region 60° - 140°. Consequently any straggling or pile-up of pulses from the scattered protons is likely to obscure the spectrum. In the first measurements taken, the α_1 group was protruding from such a continuum. The Ortec amplifier system used has a maximum count rate of 10^4 cts/sec, and as a result a good angular distribution was impossible to obtain. The discrepancies showed up at forward angles, where the yield was drastically reduced. This was due to a blocking effect in the amplifier and possibly the pulse-height analyser, caused by the increased number of scattered protons.

To remedy the situation a double delay-line amplifier was employed*, along with a voltage-sensitive preamplifier.

*Model 348, Franklin Electronics Inc., Bridgeport, Penn., U. S. A.

Clipping times of the order of 1 μs provided a good count rate tolerance. The preamplifier used was the one provided with the amplifier. It is simply a White cathode follower, but it was modified to provide a bias of 45 v to the detector by means of a battery. A 2" length of shielded cable was used to connect the preamplifier to the detector. With this instrumentation, an energy resolution of 2.1% was obtained for Am^{241} alpha particles, compared with a resolution of less than 1% for the Ortec system. The loss of resolution was due to the pulse shape obtained from the delay-line amplifier. It had a rise time of 0.5 μs, and a fall time of 0.1 μs. The pulse-height analyser requires a pulse with a rise time greater than 0.3 μs, but a fall time of 3 μs. Using a mercury pulser on the preamplifier input (coupled in with a 4.7 pf capacitor), the peak was spread out over 4-6 channels, whereas on the Ortec system equivalent pulses fell into only one channel. However, the decreased energy resolution did not affect the angular distribution data, since only the count rate tolerance of the double delay-line amplifier was required for success. The alpha group appeared typically separated from the proton background by from 2-4 channels, these channels having no counts. The group itself usually occupied a

dozen or fewer channels, so the total number of counts was easily obtained. Measurements were taken at laboratory angles from 60° to 140° inclusive, at 5° intervals, and each angle was repeated twice. The target used was the same as described in the previous section. Beam intensity was held at 0.01 μa, and the detector subtended a solid angle of 1.9×10^{-3} sr. Bombarding energy was 878 keV.

The results for this angular distribution are given in Figure II-7. They are plotted as a function of $\cos\theta_c$, and of $\cos^2\theta_c$, to exhibit fore-and-aft symmetry if it exists.

The expected angular distribution can be easily calculated using the Blatt-Biedenharn formula (Bl52)*. This method uses the channel spin formulation, in which the spin of the target nucleus and the spin of the bombarding particle combine to form the channel spin S_1. S_1 is then combined with the relative orbital angular momentum ℓ_1 of the two particles to form the spin j of the compound state. In the outgoing channel, the spin of the emitted

*For a more comprehensive review of angular distributions see Sh58 and the bibliography therein.

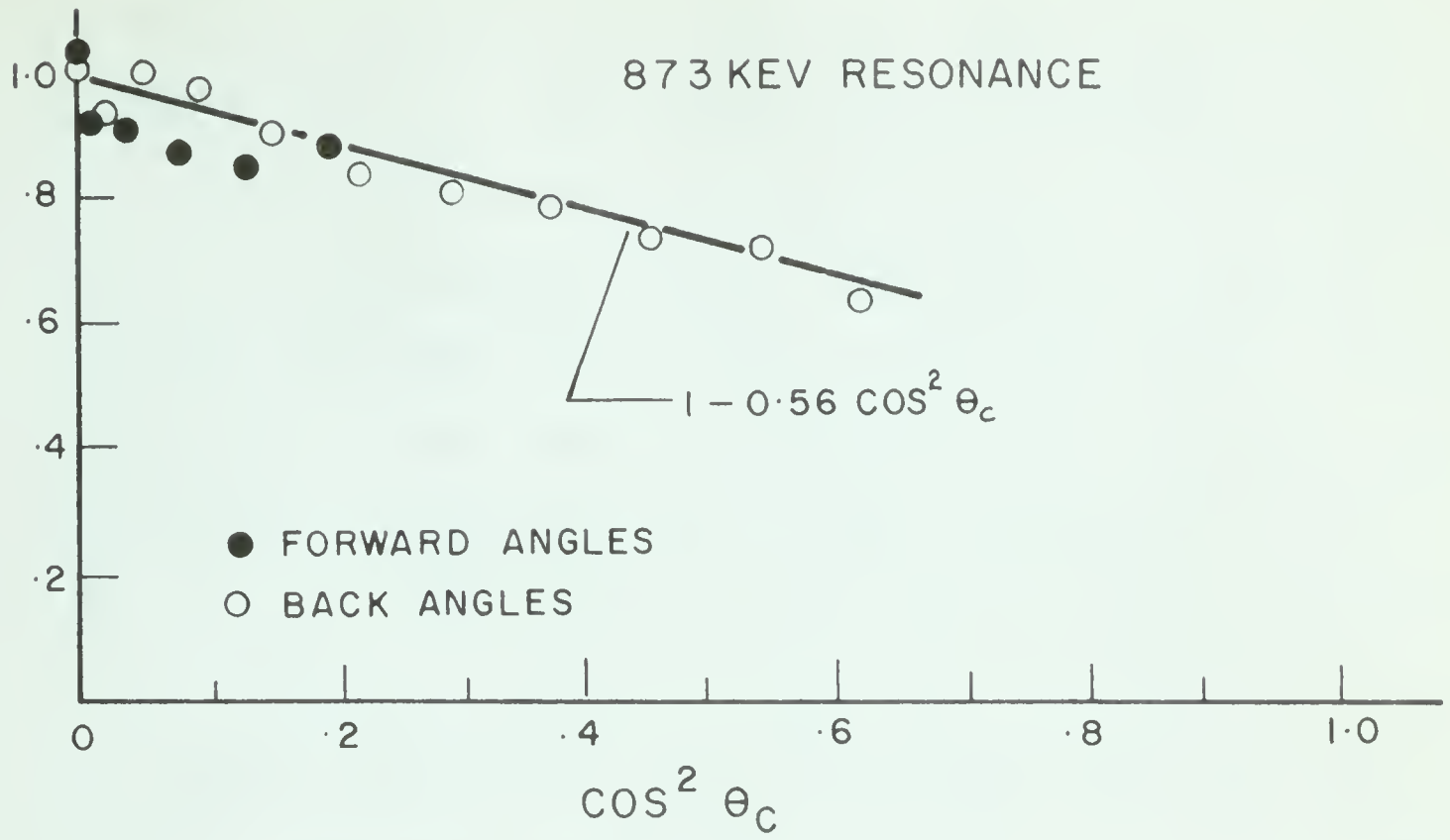

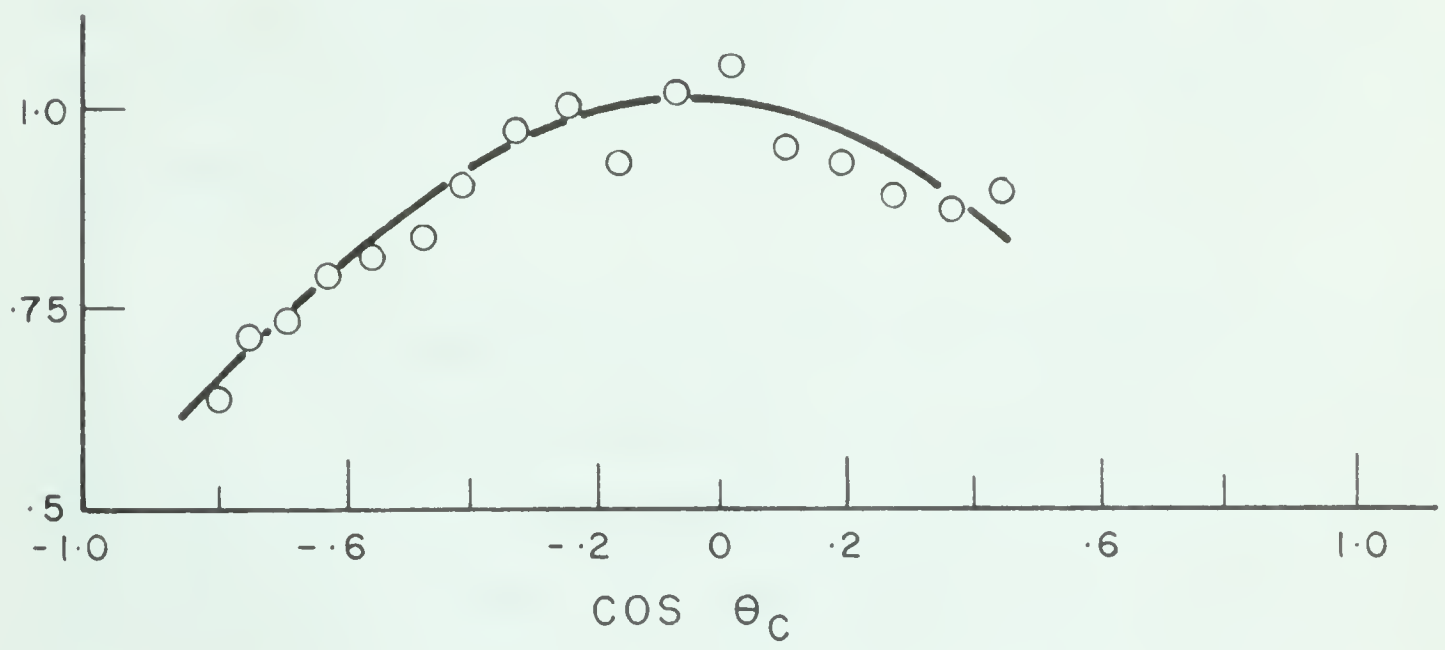

ANGULAR DISTRIBUTION OF $F^{19}(p, \alpha_1)O^{16*}$

FIG. II − 7

particle plus that of the residual nucleus forms the channel spin S_2. The orbital angular momentum ℓ_2 of the emitted particle is then added to S_2, giving the same spin j of the compound state. Of course, all angular momenta are added vectorially in the usual manner. The complexity of the angular distribution is described by a parameter k, where $k \leqslant 2\ell_1, 2j, 2\ell_2$, whichever is the smallest. If the reaction takes place through states of definite spin and parity, k must take on values 0, 2, 4---. The angular distribution of the emitted particles can then be expressed, omitting a constant, by a sum of terms:

$$W(\theta_c) \alpha \sum_{\substack{\ell_1 \ell_1' \\ \ell_2 \ell_2' \\ S_1 S_2 k}} (-1)^{S_1 - S_2} Z^o(\ell_1 j \ell_1' j, S_1 k)\, Z^o(\ell_2 j \ell_2' j, S_2 k) P_k(\cos\theta_c) \times S_{\ell_1 S_1 \ell_2 S_2}\, \overline{S}_{\ell_1' S_1 \ell_2' S_2} \qquad (9)$$

The Z^o coefficients are tabulated (see Sh54), and the S are physical matrix elements, with a bar signifying complex conjugation.

Besides depending on k, the coefficients of $P_k(\cos\theta_c)$ involve the quantum numbers $\ell_1, \ell_1', \ell_2, \ell_2'$, j, S_1 and S_2. The possibility of interference between allowed ℓ-values in both the incident and outgoing channels is taken into

account by the inclusion of primed and unprimed ℓ's. The indicated sums must include all the combinations of ℓ and ℓ'. For example, if ℓ_1 can equal 1 or 3, a given coefficent will have terms due to $\ell_1 = 1, \ell'_1 = 1$; $\ell_1 = 3, \ell'_1 = 3$; $\ell_1 = 1$, $\ell'_1 = 3$; and $\ell_1 = 3; \ell'_1 = 1$. Of course, if there is no interference, ℓ_1 always equals ℓ'_1. The permitted values for ℓ are those obtained from the triangle combination of j and the appropriate S. Different S-values do not interfere, since the channel spin is formed from two random spins.

The 13.703 MeV level in the compound nucleus Ne^{20} is involved with the resonance under consideration. It has spin and parity 2^-. The alpha particles are emitted to the 3^- 6.135 MeV level in O^{16}. Since the target nucleus F^{19} and the bombarding protons both have spin and parity $1/2^+$, the incident channel spin can take on values 0 or 1. The 0 value is excluded by parity considerations, however, because the relative orbital angular momentum ℓ_1 of the F^{19} nucleus and the proton must be odd. The emerging alpha particles are spinless, so the outgoing channel spin S_2 is 3. In the incident channel the orbital angular momentum can only be 1 or 3. Because of the low

bombarding energy, it is not unrealistic to suppress the f-wave contribution. In the outgoing channel such a simplification is not possible, and ℓ-values of 2 and 4 are permissible.

As a first approximation let us calculate the expected angular distribution considering only outgoing d-waves. In this case the Blatt-Biedenharn formula gives

$$W(\theta_c) \alpha \left[Z^o(1212,10)Z^o(2222,30) + Z^o(1212,12)Z^o(2222,32) \right.$$
$$\left. \times P_2(\cos\theta_c)\right] \left| S_{1122} \right|^2 \qquad (10)$$

This reduces to

$$\frac{W(\theta_c)}{W(90^o)} = 1 - 0.66 \cos^2\theta_c. \qquad (11)$$

In an earlier experiment, Peterson, Fowler, and Lauritsen obtained $1 - 0.49 \cos^2\theta_c$ for their distribution (Pe54). The experimental points for the present work have been fitted to a straight line by the method of least squares. This line is plotted along with the data in Figure II-7. The best-fitting line was found to be

$$\frac{W(\theta_c)}{W(90^o)} = 1 - (0.56 \pm .05)\cos^2\theta_c. \qquad (12)$$

The variance 0.05 given is the variance of the points about the line. There will be an additional error due to the variance of the points themselves (caused by the usual $\sqrt{n}$ fluctuations). As a result, the error given in Eq. 12 tends to underestimate the real situation.

Because of these uncertainties, additional calculation incorporating higher ℓ-values for the outgoing channel is not warranted. It appears that the compound system, to a good degree of approximation, is formed by p-wave protons and decays by the emission of d-wave alpha particles. Implicit here is the assumption that the spin and parity are as given, and that there is no interference from neighboring levels.

(d) $B^{11} + d$

One of the reactions presently being investigated in this laboratory is $B^{11}(d,n)C^{12}$, using time-of-flight methods to observe neutron groups to the various excited levels in the residual nucleus. Above 7.375 MeV of excitation in C^{12}, the possibility exists that it will break up into Be^{8} and an alpha particle. Experimentally, the neutron groups

to levels above 7.65 MeV are accompanied by a continuum of neutrons, possibly caused by three- or multi-body breakup of the neutron-C^{12} system. It was therefore desired to observe the charged particle spectrum from the bombardment of B^{11} by deuterons, in the hope that evidence would be uncovered which would help to determine the origin of these neutrons.

(i) Experimental Procedure

Enriched B^{11} targets* were used, nominally 99% pure. The B^{11} thicknesses were given as 100 and 60 $\mu g/cm^2$, but the material was deposited unevenly, and there were carbon deposits present from previous bombardments. Backing material was .005" tungsten and gold, respectively. Runs were first taken using the thicker target and a detector whose resolution with the Ortec system was 0.77% for 5.5 MeV alpha particles.

The target was bombarded with 0.5 MeV deuterons, the

*Obtained from A.E.R.E., Harwell, England.

detector being at a distance of two inches. Beam current was 0.13 μa. Spectra were taken at laboratory angles of 60° to 135°, at 15° intervals. The bombarding energy was then raised to 1 MeV, and the same angles repeated. This time the detector was placed five inches away, and the beam current was dropped to 0.0025 μa.

Following these experiments, the thinner target was installed, and a detector with a front dead layer of one-tenth the thickness of the first one was substituted. Its resolution for 5.5 MeV alpha particles was measured to be 0.47%. The bombarding energy was set at 526 keV, allowing for part of the target thickness, which was computed to be ~ 50 keV for 0.5 MeV deuterons. Spectra were taken at the same angles as before.

(ii) Results

A typical spectrum ($\theta_{lab} = 120^{\circ}$) obtained in the last set of bombardments is shown in Figure II-8. The large narrow peak at the left is due to $B^{11}(d,p)B^{12}$. It protrudes above the deuteron Rutherford scattering edge (not shown). Extending from this group to just below the last

CHARGED PARTICLE SPECTRUM FROM B^{11} + d

$\theta_{LAB} = 120°$ Ed = 526 KEV

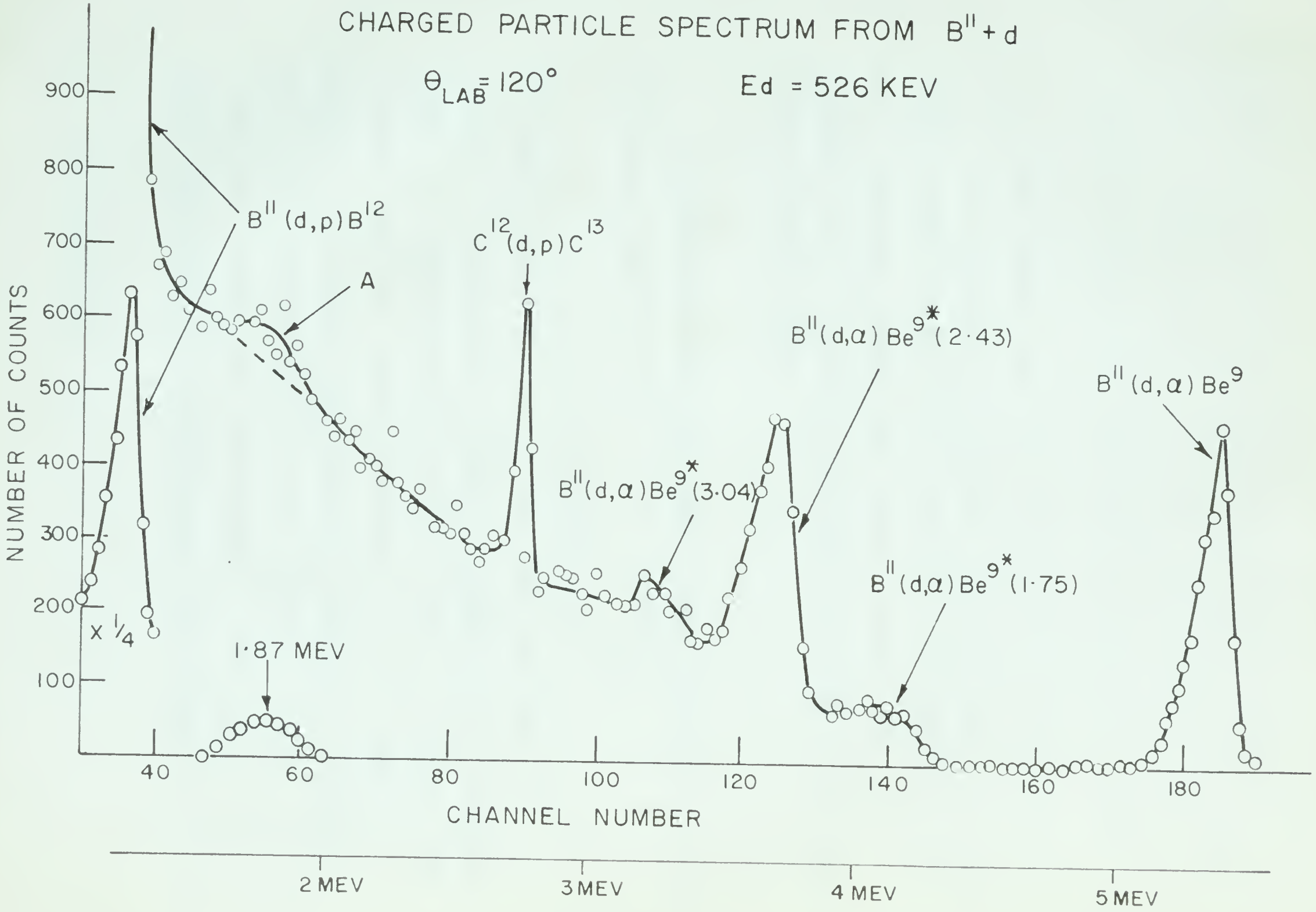

FIG. II - 8

peak is a continuum due to the multi-body reaction $B^{11} + d \longrightarrow 3\alpha + n$, and also to the breakup of the broad level in Be^{8} located at 2.9 MeV. The maximum alpha energy available from these reactions is about 5 MeV.

Superimposed upon this continuum is a "shoulder" at "A". The difference between this shoulder and the dotted curve is plotted on the axis below. The peaking at this point suggests a weak alpha group, possibly due to the breakup of C^{12*}. Similar shoulders are seen on the spectra taken at other angles.

Calculations* have been made on the kinematics of the following reaction: $B^{11} + d \longrightarrow n + C^{12*}(E_x)$

$$C^{12*}(E_x) \longrightarrow Be^{8} + \alpha$$

The alpha particle energies have been obtained as a function of laboratory detection angle, neutron emission angle, and excitation E_x of C^{12} nucleus. Of course the present experiment takes an average over all neutron angles, so no sharp alpha peaks are expected. However, the energy range covered by this shoulder ($1.87 \pm .23$ MeV) indicates evidence for the breakup of $C^{12}(9.63)$. Further work using neutron -α coincidences must be done to clarify

*See Appendix

this result. Beckner et al (Be61) also found that the 9.63 MeV level decayed by alpha emission.

The next sharp peak is due to protons from $C^{12}(d,p)C^{13}$. The C^{12} is present in a layer on the surface of the target, and is unavoidable unless a fresh target is used.

The last four peaks are due to alpha particles from $B^{11}(d,\alpha)Be^{9*}$ (3.04, 2.43, 1.75, and ground state) respectively. These groups have been observed previously by Kavanagh and Barnes (Ka58), but at a bombarding energy of 1.70 MeV. The alpha spectrum is thus obscured below an energy of 3.4 MeV, which includes the region between the two proton peaks in the present work.

Identification of the various peaks was facilitated by the good resolution of the detector. Since the protons lose much less energy in emerging from the target than do the alpha particles, there is consequently less straggling, and their peaks appear quite narrow. The shape of the alpha peaks shows the expected gently rising slope on the low energy side and a steep drop-off on the high energy side. This makes the energy of the group easy to calculate. It is given by the energy of the steep

high energy side at half-maximum, in close analogy to the procedure employed in identifying gamma-ray energies from resonances (Fo48). Allowance must also be made for the energy loss in the dead layer of the detector. The energy correction was less than 50 keV in all instances.

The data obtained at a bombarding energy of 1 MeV are less suitable for analysis, because the higher energy of the scattered deuterons obscures the spectrum. The same irregularity in the continuum appears between the two proton peaks, but identification is impossible because of poor resolution. More work using a low-noise amplifier system with a higher count-rate tolerance is presently in progress. This system should allow better resolution as well as afford more protection against pulse pile-up.

(e) Conclusions

Charged particle spectra like the one obtained by the bombardment of B^{11} by deuterons (section (d)) are very conveniently studied using the solid state detector. Unlike magnetic analysis, the whole energy range is seen at the same time, making unnecessary the normalizations

which are mandatory when the spectrum is studied a little at a time. The good resolution also enables the weaker particle groups to be observed more clearly.

The raw spectrum presented in Figure II-8 does not offer any specific information as to the origin of the neutron continuum observed in the time-of-flight measurements. The neutron-C^{12} system can break up in many different ways, all yielding the same products: three alpha particles and a neutron. It remains to investigate neutron-alpha coincidences and possibly alpha-alpha coincidences before some conclusive evidence may be obtained.

One disadvantage which did emerge during the course of the experiments is the interference caused by the Rutherford scattering of the bombarding particles. If a high energy reaction product is being studied, absorbers can be used to eliminate the lower energy particles. This procedure is only effective up to a point, however, since if alpha particles are being investigated, they lose more energy in the absorber than do protons or deuterons of the same energy. The electronics can be

improved only at the sacrifice of resolution, because the information about the energy of a particle is contained in the total charge output of the detector, and not by the slope of the current pulse's front edge. Here a compromise can be obtained by judicious choice of time constants and their place of occurrence in the amplifier. The only way to cut down on the scattering is to improve the target itself. If possible, targets should be self-supporting, or only low-Z backings should be used.

The system as it stands can be used for angular distributions and energy spectra. With a few modifications, specifically in the electronics, a significant improvement should be noted in count-rate tolerance. More elaborate experiments involving particle coincidences can then be performed with precision.

5. Appendix

Kinematics Calculation

E_1 = lab energy of deuteron (mass M_1)

E_3 = lab energy of neutron at angle θ (mass M_3)

E_4 = lab energy of C^{12} nucleus at angle φ (mass M_4)

Q_1 = Q for reaction $B^{11}(d,n)C^{12}$ = 13.731 MeV

Q_s = Energy available for neutron + C^{12} recoil

= $Q_1 - E_x$ where E_x is excitation of C^{12} nucleus.

E_α = energy of emitted α-particle in C^{12} C.M. system (mass=M_α)

E_β = energy of Be^8 nucleus in C^{12} C.M. system (mass = M_β)

Q_2 = Q for reaction $C^{12*}(E_x) \longrightarrow Be^8 + \alpha$

= E_x - 7.375 MeV

E_F = lab energy of α-particle detected at angle γ

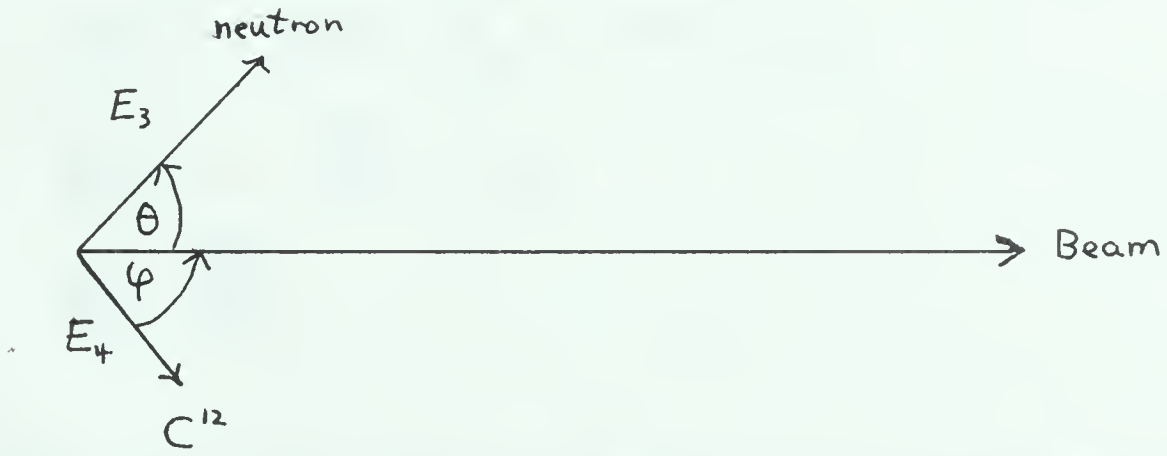

From conservation of energy and momentum,

$$E_1 + Q_s = E_3 + E_4$$

$$\sqrt{M_1E_1} = \sqrt{M_3E_3}\cos\theta + \sqrt{M_4E_4}\cos\varphi$$

$$\sqrt{M_3E_3}\sin\theta = \sqrt{M_4E_4}\sin\varphi$$

Eliminating E_4 and φ we obtain an equation from which $E_3(\theta, E_1, E_x)$ can be obtained:

$$Q_s = E_3\left(1 + \frac{M_3}{M_4}\right) - E_1\left(1 - \frac{M_1}{M_4}\right) - 2\sqrt{\frac{M_1M_3E_1E_3}{M_4}}\cos\theta$$

Eliminating E_3 and θ we get a similar equation in $E_4(\varphi, E_1, E_x)$

$$Q_s = E_3\left(1 + \frac{M_4}{M_3}\right) - E_1\left(1 - \frac{M_1}{M_3}\right) - 2\sqrt{\frac{M_1M_4E_1E_4}{M_3}}\cos\varphi$$

In the coordinate system with center-of-mass the C^{12} nucleus, we have from conservation of momentum and energy,

$$M_\alpha V_\alpha = M_\beta V_\beta$$

$$\frac{1}{2}M_\alpha V_\alpha^2 + \frac{1}{2}M_\beta V_\beta^2 = E_x - 7.375 = Q_2$$

$$\frac{1}{2}M_\alpha V_\alpha^2\left(1 + \frac{M_\alpha}{M_\beta}\right) = Q_2$$

$$V_\alpha^2 = \frac{4Q_2}{3M_\alpha}$$

We then add this velocity vectorially to the velocity

of the C^{12} nucleus to obtain the velocity of the α-particle in the lab system at angle γ. For simplicity let all reactions take place in the plane of the beam and the neutron and alpha detectors.

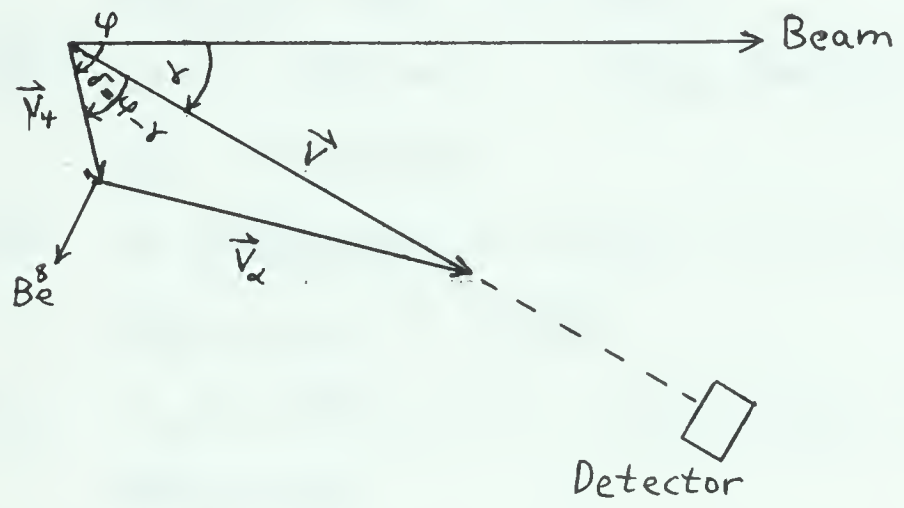

$$E_F = \frac{1}{2}M_\alpha V^2$$

$$E_4 = \frac{1}{2}M_4 V_4^2$$

$$\frac{2Q_2}{3} = \frac{1}{2}M_\alpha V_\alpha^2$$

$$V_\alpha^2 = V^2 + V_4^2 - 2VV_4\cos\delta \quad \text{where } \delta = \varphi - \gamma.$$

Finally we obtain

$$\sqrt{E_F} = \sqrt{\frac{M_\alpha E_4 \cos^2\delta}{M_4}} \pm \sqrt{\frac{M_\alpha E_4}{M_4}(\cos^2\delta - 1) + \frac{2Q_2}{3}}$$

In all cases of interest the + sign is the only significant one.

E_F has been calculated using the IBM 1620, for $\theta = 0$ to 180° in 15° intervals, $\gamma = 0$ to 180° in 15° intervals, all C^{12} excitations from 7.65 to 14.05, and deuteron bombarding energies of 0.5, 1.0, 1.4 and 1.5 MeV.

REFERENCES

A160 W. D. Allen, in "Fast Neutron Physics", J. B. Marion, J. L. Fowler, Ed., Interscience (1960) p 362ff

A161 T. K. Alexander, F. S. Goulding, Nuclear Instr. & Methods, 13, 244 (1961)

An62 J. D. Anderson, C. Wong, Nuclear Instr. & Methods, 15, 178 (1962)

Ba60 E. Baldinger, W. Czaja, A. Z. Farooqi, Helv. Phys. Acta, 33, 551 (1960)

Bl52 J. M. Blatt, L. C. Biedenharn, Rev. Mod. Phys. 24, 249 (1952)

Bl60 J. L. Blankenship, C. J. Borkowski, IRE Trans. in Nuclear Science, NS-7, 190 (1960)

Bl61 J. L. Blankenship, C. J. Borkowski, IRE Trans. in Nuclear Science, NS-8, 17 (1961)

Br59 F. D. Brooks, Nuclear Instr. & Methods, 4, 151 (1959)

Br60 J. E. Brolley, J. L. Fowler, in "Fast Neutron Physics", J. B. Marion, J. L. Fowler, Ed., Interscience (1960) p 80-81

Br61 W. L. Brown, IRE Trans. in Nuclear Science, NS-8, 2 (1961)

Da61 W. Daehnick, R. Sherr, Rev. Sci. Instruments, 32, 666 (1961)

De60 A. J. Dekker, "Solid State Physics ", (Prentice-Hall) 1960 p307

De61 G. Dearnaley, A. B. Whitehead, Nuclear Instr. & Methods, 12, 205 (1961)

Ga61 E. Gatti, F. de Martini, Conference on Nuclear Electronics, Paper #NE/67 (Belgrade 1961)

Go59 F. S. Goulding, L. B. Robinson, "A Transistor Trigger Circuit Exhibiting an Accurate Triggering Threshold". Chalk River Report CREL-778 (1959)

Hu58 "Neutron Cross Sections", 2nd Ed., D. J. Hughes, R. Schwartz, BNL report #325, (1958) p 74

Hu60 "Neutron Cross Sections", 2nd Ed., D. J. Hughes, R. Schwartz, BNL report #325, Supplement #1 (1960) p 108

Is58 A. Isoya, H. Ohmura, T. Momota, Nuclear Physics, 7, 116 (1958)

Is58a A. Isoya, Nuclear Physics, 7, 126 (1958)

Ka58 R. W. Kavanagh, C. A. Barnes, Phys. Rev. 112, 503 (1958)

Kl61 R. W. Klingensmith, IRE Trans. in Nuclear Science, NS-8, 112 (1961)

Li59 A. E. Litherland, E. Almquist, R. E. Batchelor, H. E. Gove, Phys. Rev. Letters, 3, 104 (1959)

Ma54 J. B. Marion, A. S. Ginzbarg, Tables for the Transformation of Angular Distribution Data from the Laboratory System to the Center of Mass System, Shell Development Co. #NP-6241 (1954)

Ma60 J. B. Marion, J. L. Fowler, Ed., "Fast Neutron Physics", Interscience (1960) 608-616, 228-245, Bibliography on p 245

Ma 62 J. W. Mayer, IRE Trans. in Nuclear Science, NS-9, 124 (1962)

Ne60 G. C. Neilson, W. K. Dawson, J. T. Sample, F. A. Johnson, Suffield Technical Paper #176, 22 (1960)

Ne60a G. C. Neilson, W. K. Dawson, J. T. Sample, F. A. Johnson, Suffield Technical Paper #176, 11 (1960)

Ow58 R. B. Owen, IRE Trans. in Nuclear Science, NS-5, 198 (1958)

Pe54 R. W. Peterson, W. A. Fowler, C. C. Lauritsen, Phys. Rev. 96, 1250 (1954)

Ra61 C. T. Raymo, J. W. Mayer, IRE Trans. in Nuclear Science, NS-8, 157 (1961)

Ru47 S. Rubin, Phys. Rev. 72, 1176 (1947)

Sh54 W. T. Sharp, J. M. Kennedy, B. J. Sears, M. G. Hoyle, "Tables of Coefficients for Angular Distribution Analysis", Chalk River Report CRT-556 (1954)

Sh58 W. T. Sharp, "The Quantum Theory of Angular Momentum", Chalk River Report CRL-43 (1958)

To61 P. A. Tove, K. Falk, Nuclear Instr. & Methods 12, 278 (1961)

Vr61 L. de Vries, F. Udo, "A Fast Pulse-Shape Discriminator with Applications as a Spectrometer and Sensitive Monitor for 1-30 MeV Neutrons. Preprint from Institute for Nuclear Physics Research Amsterdam, Netherlands (1961)

Wr56 G. T. Wright, Proc. Phys. Soc., 69B, 358 (1956)

Be61 E. H. Beckner, C. M. Jones, G. C. Phillips, Phys. Rev. 123, 255 (1961)